NASA Contractor Report 172426

Fault-Tolerant System Considerations for a Redundant Strapdown Inertial Measurement Unit

Paul Motyka, Renato Ornedo, Rami Mangoubi
THE CHARLES STARK DRAPER LABORATORY, INC.
555 Technology Square
Cambridge, Massachusetts 02139

NASA

National Aeronautics and
Space Administration

Langley Research Center
Hampton, Virginia 23665

LIST OF TABLES

LIST OF TABLES (Concluded)

LIST OF SYMBOLS

$\underline{a}$ vector of elements of A matrix arranged in row sequence

$\bar{A}$ VH_m with elements $\bar{A}_{ij}$

Ai, Bi   two input axes of instruments, i = 1,2,3,4

b, b_1, b_2 magnitude of bias failure (rad or m/s)

c.g.   vehicle center of gravity

C_ρ covariance matrix of parity equation residuals (rad^2 or $(m/s)^2$)

C_i contribution of error source i to C_ρ, i = 1,2,...,K

d   distance from c.g. to sensor location with components d_x, d_y, d_z (m)

D_j degree of inconsistency for sensor j's measurement

DF_D failure detection decision function (rad^2 or $(m/s)^2$)

DF_{I_j} failure isolation function for the jth sensor (rad^2 or $(m/s)^2$)

DT   computation time interval (sec)

$\underline{e}_i$ error vector due to ith sensor error, i = 1,2,...,k

E   expected value operator

F_{ij} logical variables in edge vector algorithm used to detect and isolate failures in instruments i and j, i,j = 1,2,3,4

FS	fuselage station from nose of aircraft
G_i	logical variable indicating sensor i's failure when on
G_ϕ	gravitational constant (9.8062 m/s^2/g (32.1725 ft/s^2/g))
H	sensor configuration geometry matrix
H_m	geometry matrix of scale factor and misalignment errors
I	identity matrix
m	sensor outputs (rad or m/s)
n	number of sensors or states
n_x, n_y, n_z	longitudinal, lateral, and normal body-axes linear inertial accelerations (g)
$n_{z_{\eta_i}}, n_{y_{\eta_i}}$	coefficients relating effect of vehicle structural modes on linear accelerations, i = 1,2,...,6 (g-s^2)
p, q, r	body axes roll, pitch, yaw rates (rad/s)
$\dot{p}_{\eta_i}, \dot{q}_{\eta_i}, \dot{r}_{\eta_i}$	coefficients relating effect of vehicle structural modes on angular rates, i = 1,2,...,6 (rad)
R_i	covariance matrix of $\underline{e}_i$
S_{g_i}	g sensitivity of ith instrument input axis
S_i	spin axis of instrument i, i = 1,2,3,4
t	time in seconds (s)
T	failure-detection threshold (rad^2 or (m/s)^2)
V	(n-3)×n matrix of parity equations
V_j	jth column of V

x, y, z	body axes system components
x_o	offset of IMU from vehicle centerline (m)
x_s	separation of IMU1, IMU2 from IMU centerline (m)
α	$\dfrac{\sqrt{3} - 1}{2\sqrt{3}}$
α_{IP}	accelerometer input-pendulous-axes cross-coupling error (g/g^2)
β	$\dfrac{\sqrt{3} + 1}{2\sqrt{3}}$
β_{II}	accelerometer input-axis-squared error (g/g^2)
γ	$1/\sqrt{3}$
δDF_D	change in failure decision function due to bias failure $(rad^2$ or $(m/s)^2)$
δm	composite sensor error term (rad or m/s)
δn	incremental acceleration error due to structural mode and lever arm effects (g)
ε	scale-factor error (rad)
$\underline{\varepsilon}_i$	$V\underline{e}_i$, effect of sensor uncertainty on the parity equation residual
ζ	measurement noise which is Gaussian with zero mean
η_i	generalized bending mode coefficients, $i = 1, 2, \ldots, 6$
λ	bias error (deg/hr or g)
μ	misalignment error (rad)

ρ GLT parity equation residuals (rad or m/s)

ρ_c correlation coefficients between axes of two degree of freedom instrument

σ standard deviation of the instrument noise (rad or m/s)

σ_1^2 sum of squares of 1σ value of bias, hysteresis, etc.

$\sigma_{S_g}^2$ variance of S_g

ω three-dimensional vector of body-axes inertial linear accelerations (m/s) or angular rates (rad)

Ω skew symmetric form of ω

Superscripts

-1   inverse

p   pendulous axis

T   transpose

^   estimated value

Subscripts

a   accelerometer

B   structural mode effects included

f   filtered

F   presence of failed sensor

i,j,k	element number, row and/or column indicator of vectors or matrices
la	lever arm effects
L	left
m	positive maximum or upper bound
MIS	misalignment
N	absence of failed sensor
NOISE	noise
R	right
SE	sensor error
SF	scale factor
SM	structural mode and lever arm

SECTION 1

INTRODUCTION

One way to lower the cost of aircraft and improve system reliability is to integrate the avionics functions. There is presently considerable interest in replacing the multiple sensors of a typical modern commercial aircraft with a skewed array of strapdown inertial navigation sensors. Redundant computers are used to perform multiple functions such as flight control, air-data processing, and strapdown navigation. Net cost has been shown to be less than for the current non-integrated systems. The integrated avionics approach depends upon redundancy to achieve the required reliability. Because flight control, system reliability and safety depend upon integrated avionics reliability, thorough analysis of skewed sensor system reliability is essential.

The present study was undertaken within the context of this framework. It involved the evaluation and analysis of the Redundant Strapdown Inertial Measurement Unit (RSDIMU) being developed and evaluated by the NASA Langley Research Center. The work was conducted by The Charles Stark Draper Laboratory, Inc. (CSDL) under NASA Contract NAS1-16887 entitled the False Alarm/Reliability Analyses for a Separated Dual-Fail Operational Redundant Strapdown Inertial Measurement Unit. It is a follow-on to previous efforts described in References 1 and 2. The goal of the initial effort was to assess the feasibility of performing failure detection and isolation (FDI) for the RSDIMU in an air transport environment, develop and evaluate FDI algorithms for the RSDIMU, and analyze FDI system performance. In Reference 2, a methodology for quantitatively analyzing the reliability of redundant avionics systems in general and

1

the dual, separated RSDIMU system in particular is developed and applied using a Markov model reliability analysis tool. The results of the parametric study of significant instrument and FDI system variables are presented and discussed.

The detection and isolation of failures of the dual, separated RSDIMU is accomplished by comparing a function of the sensor outputs with a threshold. The separation of the RSDIMU into two separated clusters severely complicates the selection of the thresholds. The incremental structural mode and accelerometer lever arm effects between the locations of the two instrument clusters must be taken into account. In Reference 2, a technique is developed and analyzed for generating the thresholds for a dual, separated RSDIMU taking into account factors such as the sensor errors, the aircraft dynamic environment, accelerometer lever arm effects and vehicle structural modes.

The present effort was conducted to further develop and refine the technical knowledge and skills needed to make redundant strapdown IMUs a viable component of the aircraft avionics system inventory. Two major efforts were undertaken. The first was an Aeroelastic Effects Analysis, the major goal of which was to develop a methodology to determine the effects of aircraft aeroelasticity on gyro and accelerometer FDI system capability. Particular emphasis was placed on determining the effects and sensitivity of FDI system capability to the mounting location of a physically separated RSDIMU. Another of CSDL's goals with regard to this subject was to develop and evaluate a technique for generating FDI system thresholds which account for aeroelastic effects and which are valid for multiple, nonconcurrent failures. CSDL's deterministic digital aircraft simulation was used to assess the impact of the aeroelastic effects on the capability of the FDI system and evaluate the effectiveness of the method developed for generating the dynamic thresholds.

CSDL also investigated the concept of Failure Decision Function Compensation. The goal of this task was to account for the vehicle environment by compensating the failure decision function by the parity

2

residual error covariance (Reference 3). The major intent is to assess the feasibility of this approach and compare it with the dynamic threshold compensation method. The method to be investigated uses the Generalized Likelihood Test (GLT) with a more general form of the failure decision and isolation functions than has been considered in the previous phases of this study.

The report is organized as follows. Section 2 contains background information regarding the results of previous work conducted by the C.S. Draper Laboratory with regard to the RSDIMU. A comparison of Generalized Likelihood Test FDI algorithms is contained in Section 3. The comparison is made between failure decision functions which are compensated for sensor errors or else normalized with respect to them. The intent of this section is to determine if the use of compensated decision functions can eliminate the need for the dynamic failure detection thresholds required with the normalized decision function. Section 4 contains a discussion of noise compensation in the thresholds of the FDI GLT algorithm, a subject which has not been addressed up to this point in the consideration of the RSDIMU but which is shown to be necessary to eliminate false alarms. A consideration of the effects of sensor location and magnitude of the structural modes on FDI system performance is presented in Section 5. This topic is significant since the designers of aircraft systems using an RSDIMU will have to account for these factors. Section 6 is devoted to the development and analysis of an algorithm for generating the failure detection thresholds of the GLT algorithm using noise compensation and filtered parity equation residuals. The latter is a method of obtaining exact compensation of the high frequency structural mode and accelerometer lever arm effects. Section 7 presents an FDI strategy based on the pairwise comparison of sensor measurements. This strategy uses GLT derived detection decision functions. It has the specific additional advantage of successfully detecting and isolating up to two simultaneously occurring failures. The limitations of this advantage are also demonstrated. Finally, the contents of this report are summarized and the major conclusions are presented in Section 8.

SECTION 2

BACKGROUND

2.1   Sensor Configuration

The inertial measurement unit shown in Figure 1 is a redundant strapdown package employing four two-degree-of-freedom (TDOF) gyros (accelerometers) in a semi-octahedral geometry. The instruments are positioned such that the spin (pendulous) axes are normal to the four faces of the semi-octahedron and point out. The two measurement axes of the gyros and accelerometers lie in the plane of the face and are symmetric about the face centerline. The RSDIMU consists of two separate packages (faces 1 and 2, faces 3 and 4) which may be spatially separated along a track in the lateral direction. Thus it may be treated as two tetradic IMUs as indicated in Figure 2. The reason for separating the RSDIMU into two halves is to provide protection against damage effects due to lightning, structural failure, etc. The benefits of redundancy in the form of improved system reliability are retained by using sensor information from both halves of the IMU for failure detection and isolation purposes.

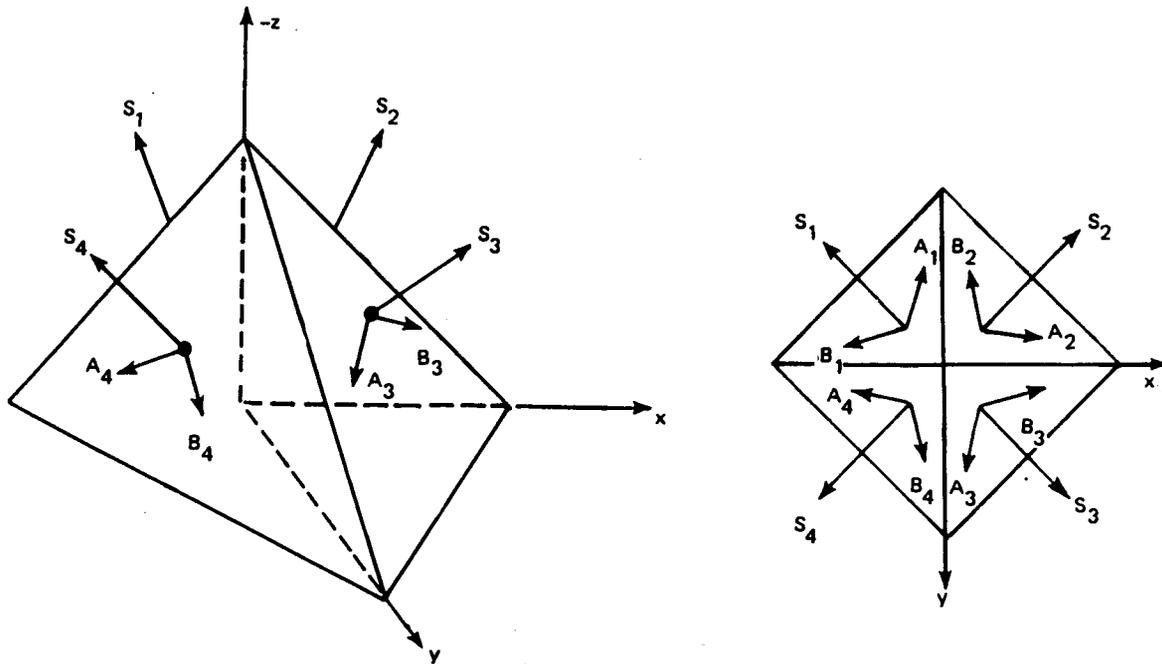The nominal geometry matrix, defining the sensor input axes relative to the vehicle body axes is

Figure 1. RSDIMU Instrument Geometry

x_o, OFFSET OF IMU FROM VEHICLE CENTERLINE

x_s, SEPARATION OF IMU1, 2 FROM IMU CENTERLINE
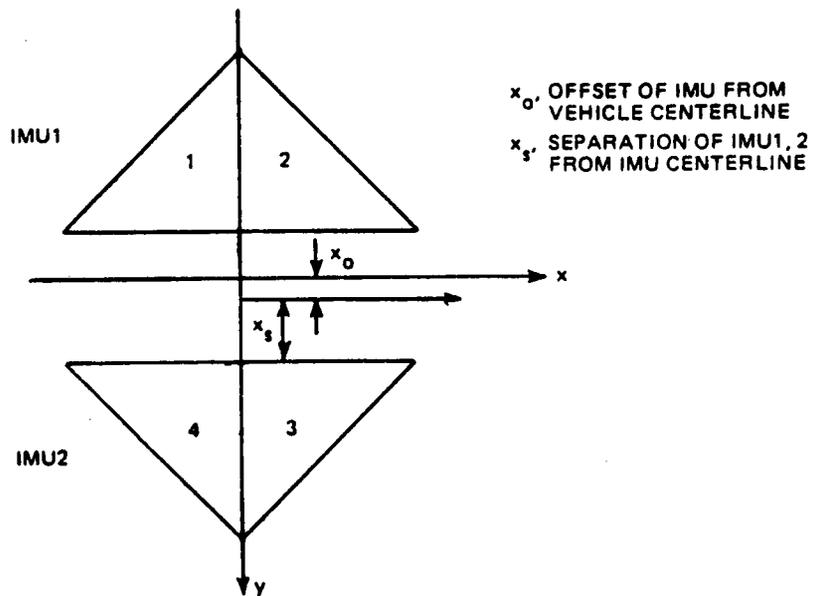
Figure 2. Separation of Sensor Configuration into Two IMUs

$$
H = \begin{bmatrix}
\alpha & -\beta & \gamma \\
-\beta & \alpha & \gamma \\
\beta & \alpha & \gamma \\
-\alpha & -\beta & \gamma \\
\hdashline
-\alpha & \beta & \gamma \\
\beta & -\alpha & \gamma \\
-\beta & -\alpha & \gamma \\
\alpha & \beta & \gamma
\end{bmatrix}
$$

where

$$
\alpha = \frac{\sqrt{3} - 1}{2\sqrt{3}}
$$

$$
\beta = \frac{\sqrt{3} + 1}{2\sqrt{3}}
$$

$$
\gamma = \frac{1}{\sqrt{3}}
$$

The dashed line indicates the separation of the RSDIMU into two halves. The nominal sensor error parameters used in this study are presented in Table 1.

2.2   General Concepts of FDI

This section is included to provide the reader with a background in the general concepts applied to detect and isolate sensor failures. It will allow a greater understanding and appreciation of the material presented in the following sections of the report.

In order to detect and isolate sensor failures, a system of parity equations is solved. Parity equations are linear combinations of the

Table 1
Nominal Sensor Parameters

PARAMETER	VALUE
Gyros	
Bias	0.01 deg/hr
Scale Factor Error	20.0 ppm
Misalignment	50.0 μrad
g Dependent Errors	0.005 deg/hr/g
g^2 Dependent Errors	0.02 deg/hr/g^2
ω^2 Dependent Errors	12.4 deg/hr/(rad/sec)^2
Accelerometers	
Bias	50 μg
Scale Factor Error	50 ppm
Misalignment	50.0 μrad
Input-Pendulous Axes Acceleration Sensitivity Coefficient	70 μg/g^2
Input Axis Accelerometer Squared Sensitivity Coefficients	20 μg/g^2

sensor outputs selected to enhance the uncertainties (failures) associated with the sensors. Furthermore, the effects of the quantity which the instruments measure, i.e., the angular rates or linear accelerations, are removed from consideration by the parity equations.

Failure detection occurs as a result of comparing the parity equation residuals or a function of them to a threshold. If the threshold is exceeded, a failure is declared and the failure is then isolated. Failure isolation is accomplished using the parity equation residuals. Several methods are used depending upon the algorithm employed. Logical operations based on the residuals which exceed the threshold is one technique used, e.g., a combination of residuals exceeding the thresholds indicates the failure of a particular sensor. Another approach involves the dot product of the vector of parity equation residuals with vectors defined by the coefficients of the parity equations to isolate a failure.

This, in essence, is the methodology applied to detect and isolate sensor failures. However, complications arise when it is applied to a practical situation. For example, the parity equation residuals are ideally zero when a failure is not present and nonzero when a failure has occurred. In reality, the residuals are nonzero because of the uncertainties associated with the sensors, i.e., the sensor errors, sensor noise, structural mode effects, accelerometer lever-arm effects, etc. The residuals due to these factors dictate the level of failure which can be detected since they do not arise from failures and are a result of normal, although undesirable, sensor behavior. In a dynamic environment these uncertainties may be excited to a greater degree. To avoid the false detection of failures, i.e., false alarms, the thresholds may have to be compensated for this effect. One possible approach to handling this problem is the use of dynamic thresholds which are a function of the environment. Another is in-flight identification and compensation of the sensor error effects in the FDI decision process.

Normally, unfiltered sensor data is used to detect and isolate sensor failures of a large magnitude since it is desired to remove their

effects before they affect the controllability of the vehicle. Another factor in the design of FDI systems is that the effects of small magnitude failures may be masked by the instrument uncertainty effects. Filtering of the parity equation residuals may have to be introduced into the FDI system to enhance their detectability. This is at the expense of a longer detection time and a design tradeoff exists. The presence of several channels in the FDI system to detect and isolate different levels of failures may result.

2.3 Description of the Generalized Likelihood Test Failure Detection and Isolation Algorithm

The Generalized Likelihood Test Failure Detection and Isolation algorithm has been used during this study. A brief description of it follows. Three levels of failure are to be detected and isolated. They are:

- Hard failures: those of a comparatively large magnitude, which primarily affect flight-control performance.

- Midvalue failures: those of medium magnitude, which affect pilot display performance.

- Soft failures: those of a comparatively small magnitude, which affect navigation performance.

Consider first the hard failure channel. In the absence of sensor failures, the measurement equation is

$$m = H\omega + \zeta$$

A set of parity equations is defined by

$$\rho = Vm$$

where

$$VH = 0$$

V is assumed to be of dimension (n-3)×n. The matrix V can be chosen so that

$$VV^T = I$$

Combining the previous equations yields

$$\rho_N = V\zeta$$

In the absence of sensor failures, ρ_N depends only on the measurement noise. If sensor j experiences a bias-type failure and that failure is manifest as an apparent bias shift of magnitude b in measurement j, then

$$\rho_F = V\zeta + V_j b$$

The difference in the statistics of ρ_N (in the absence of failures) and ρ_F (in the presence of failures) provides a basis for detecting and isolating failures. The problems of detecting and isolating sensor failures fall within the general framework of composite hypothesis tests, since the sign as well as the magnitude of the bias failure is unknown a priori.

A GLT formation of the detection and isolation problems has been developed. Assume single-axis failures for simplicity. The GLT decision functions for detection and isolation are

$$DF_D = \rho^T C_\rho^{-1} \rho \tag{1}$$

$$DF_{I_j} = \frac{\left(\rho^T C_\rho^{-1} v_j\right)^2}{v_j^T C_\rho^{-1} v_j} \quad , \quad j = 1,2,\ldots,n \tag{2}$$

11

The detection decision is made by comparing DF_D to a detection threshold. A sensor failure results in a change in the mean value of a sensor output, the parity-equation residuals, and the failure-detection function. The isolation decision is then made by determining $\max_j(DF_{I_j})$. The value of j that maximizes DF_{I_j} identifies the sensor that is most likely to have failed.

The form of the failure detection and isolation functions presented in the previous paragraph is more general than that used in the prior studies of the RSDIMU in that the effect of C_ρ is included. Decision functions, normalized to remove the effect of C_ρ, have been investigated previously. A comparison of these two decision function forms is presented in Section 3.

The detection and isolation of the mid and soft failures is accomplished using the same decision functions as for the hard-failure channel. The only exception is that the appropriately filtered parity-equation residuals are used in lieu of the unfiltered ones. Figure 3 is a block diagram of the FDI which has evolved during this program.

2.4   System Simulation and Evaluation Trajectories

A digital aircraft simulation was used during this study to evaluate the technical areas and tasks of the Statement of Work. A block diagram of the simulation used is shown in Figure 4. The core of the simulation is a six-degree of freedom aircraft model with nonlinear aerodynamics. Also modeled are a flight control system and turbulence. An autopilot "commands" the vehicle to follow a desired trajectory profile. Skewed gyro and accelerometer sensor configurations are modeled with the location of the sensors variable to permit an assessment of accelerometer lever-arm effects. The sensors are assumed to be of navigation quality and used for navigation and flight control purposes. The FDI algorithm operates on the sensor data to generate the input signals to the flight control and navigation systems. Navigation accu-
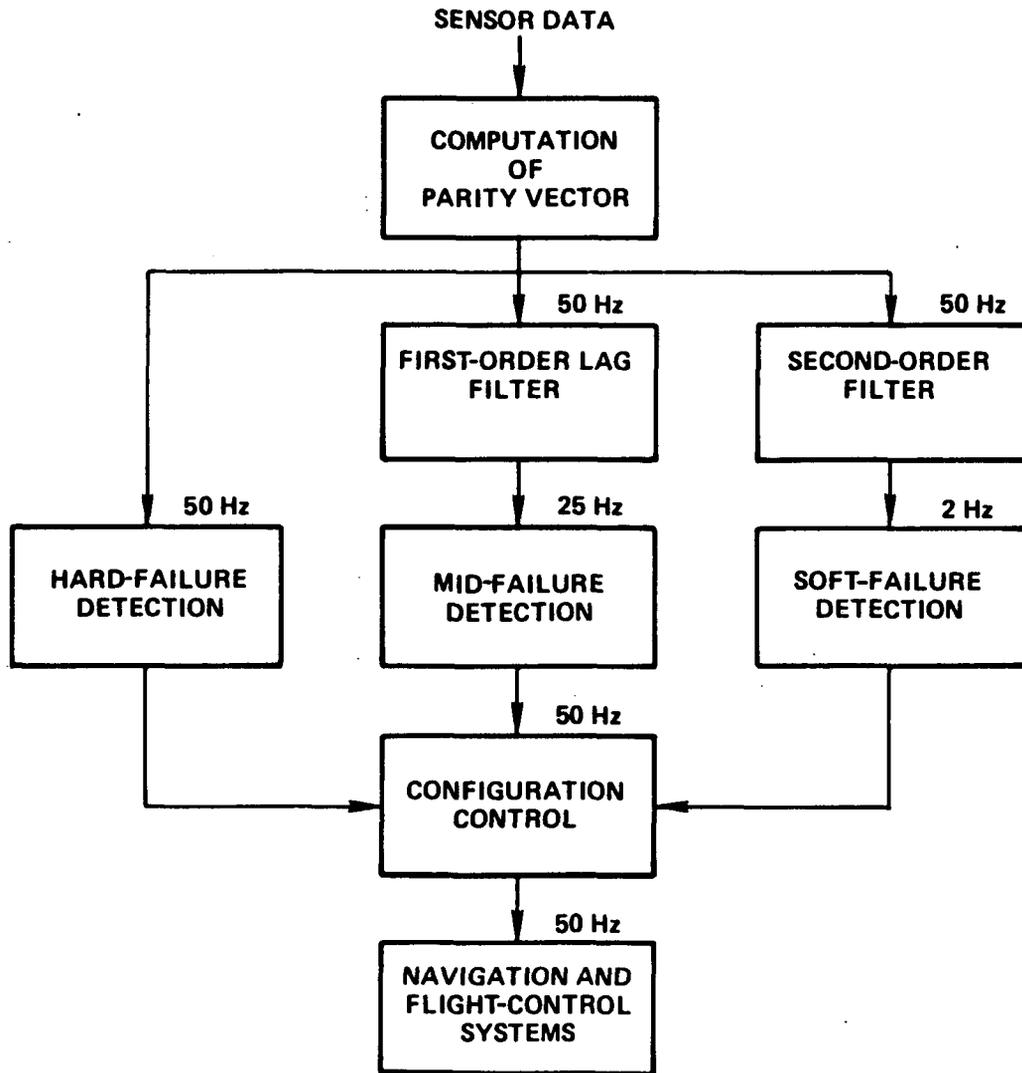
12

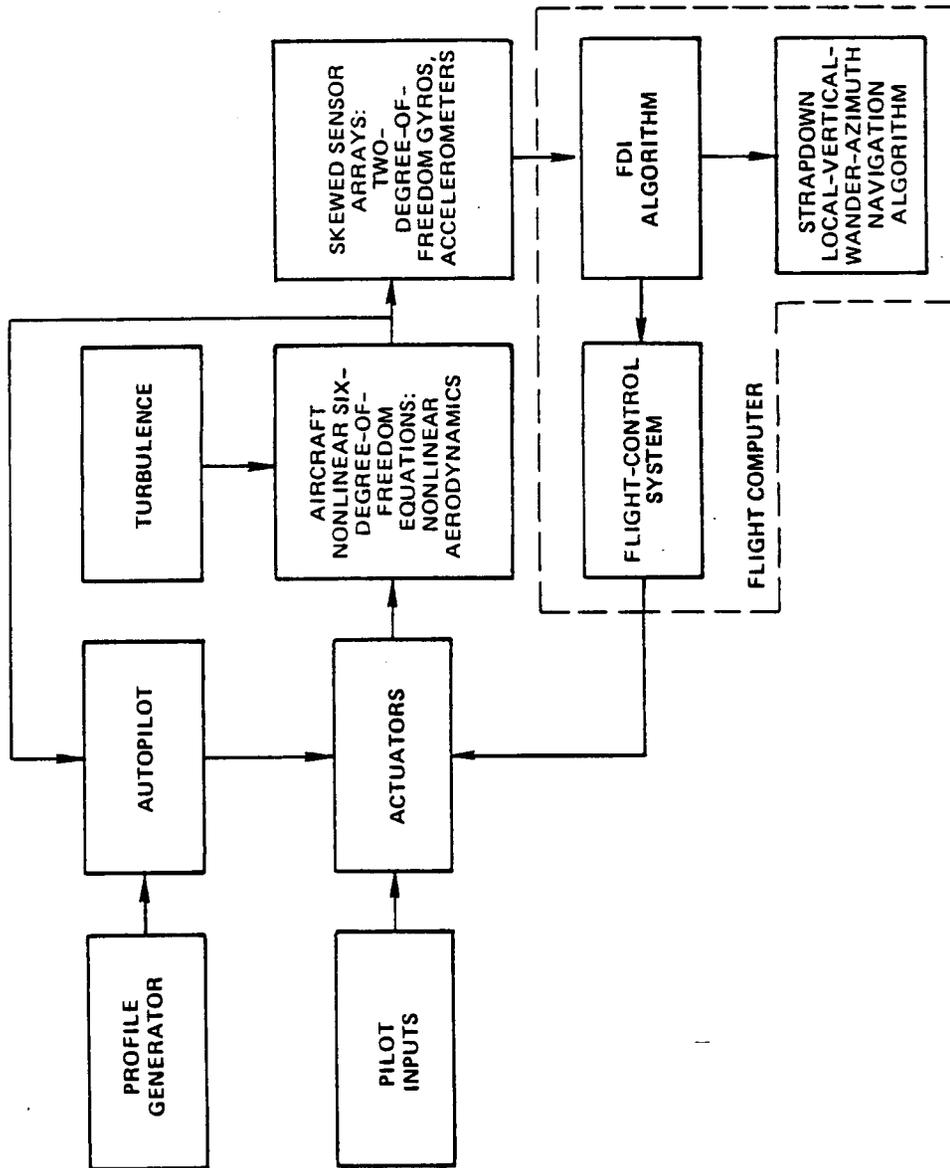Figure 3. FDI Algorithm Block Diagram

Figure 4. Simulation Block Diagram

racy is assessed by differencing the outputs of a strapdown local-vertical-wander-azimuth navigation system model and the vehicle states.

Table 2 shows the longer of the two flight profiles used to evaluate the fault-tolerant system during the dynamic phases of vehicle flight. The profile includes features from a typical transport aircraft mission profile: a climb to altitude, cruise, heading changes, descent, and a loiter maneuver. Shorter 110 seconds and 500 second profiles were also used during this study. The 110-second profile is outlined in Table 3, and the 500-second profile is all-cruise.

2.5   Separated Sensor Effects

The present program is concerned with the development and evaluation of an analytic technique for the generation of FDI thresholds for an aircraft system with dual, separated IMUs. The intent is to use all available instruments of both IMUs to detect and isolate sensor failures. The separation of the IMUs hinders failure detection and isolation, since the raw structural-mode and accelerometer lever-arm effects which the instruments sense are comparable in magnitude to the failures which may be encountered and can result in the false detection of failures if not properly accounted for. The selection of thresholds, a major consideration in the development of any FDI system, is especially complicated when separated, communicating IMUs are present, since these additional factors must be taken into account. A spectrum of failure magnitudes from hard through soft is considered. Finally, aircraft maneuvering adds a significant dimension to the problem. The structural-mode and accelerometer lever arm effects are now defined.

2.5.1 Structural-Mode Effects

Each structural mode can be represented by a second-order differential equation with additional terms which, in general, couple in the basic rigid-body airframe response, the other modes, and the control-surface deflections. The effect of the structural modes on the

15

Table 2
30 Minute Evaluation Trajectory

TIME (sec)	EVENT	ALTITUDE (m)	VELOCITY (m/sec)
0 - 50	Cruise	1497	166
50 - 300	Ascent		
300 - 500	Cruise	3974	205
500 - 550	10° Heading Change		
550 - 750	Descent		
750 - 765	10° Heading Change		
765 - 1000	Cruise	1497	166
1000 - 1015	10° Heading Change		
1015 - 1105	Cruise		
1195 - 1705	Loiter, one 360° turn		
1705 - 1800	Cruise	1497	166

Table 3
110 Second Flight Trajectory

TIME (sec)	EVENT
0 - 40	Cruise
40 - 100	3 deg/min Climb
	20 deg/min Bank
	90 deg/min Heading Change
110 - 110	Cruise, 20 deg Bank Angle

angular rates and linear accelerations is a function of sensor locations and is indicated by the following equations.

$$p_B = p + \delta p_B = p + p_{\dot{n}_4} \dot{n}_4 + p_{\dot{n}_5} \dot{n}_5 + p_{\dot{n}_6} \dot{n}_6$$

$$q_B = q + \delta q_B = q + q_{\dot{n}_1} \dot{n}_1 + q_{\dot{n}_2} \dot{n}_2 + q_{\dot{n}_3} \dot{n}_3$$

$$r_B = r + \delta r_B = r + r_{\dot{n}_6} \dot{n}_6$$

$$n_{y_B} = n_y + \delta n_{y_B} = n_y + n_{y_{\ddot{n}_6}} \ddot{n}_6$$

$$n_{z_B} = n_z + \delta n_{z_B} = n_z + n_{z_{\ddot{n}_1}} \ddot{n}_1 + n_{z_{\ddot{n}_2}} \ddot{n}_2 + n_{z_{\ddot{n}_3}} \ddot{n}_3 \qquad (3)$$

2.5.2 Accelerometer Lever-Arm Effects

The linear accelerations measured at a distance d meters from the c.g. of the vehicle (in terms of the linear accelerations at the c.g. of the vehicle and the accelerometer lever-arm effects) are defined by the following equations.

$$
\begin{aligned}
n_{x_d} &= n_{x_{cg}} + \delta n_{x_{\ell a}} \\
&= n_{x_{cg}} + \frac{1}{G_\phi} \cdot \left[-(q^2 + r^2)d_x + (qp - \dot{r})d_y + (\dot{q} + pr)d_z \right]
\end{aligned}
$$

$$
\begin{aligned}
n_{y_d} &= n_{y_{cg}} + \delta n_{y_{\ell a}} \\
& n_{y_{cg}} + \frac{1}{G_\phi} \cdot \left[(\dot{r} + pq)d_x - (p^2 + r^2)d_y + (rq - \dot{p})d_z \right]
\end{aligned}
$$

18

$$n_{z_d} = n_{z_{cg}} + \delta n_{z_{\ell a}}$$

$$= n_{z_{cg}} + \frac{1}{G_\phi} \cdot \left[(pr - \dot{q})d_x + (qr + \dot{p})d_y - (p^2 + q^2)d_z \right] \quad (4)$$

2.6   The Derivation of Dynamic Thresholds

The basic approach is to start with an analytic expression for the sensor error, structural-mode, and lever-arm effects and obtain expressions for the parity-equation residuals. Upper bounds for the parity-equation residuals are then determined. The FDI system threshold is generated by duplicating the steps involved in the computation of the failure-decision function using the upper bounds for the parity-equation residuals rather than the actual residuals. A block diagram of the process for the mid or soft failure channel is shown in Figure 5.

It is necessary to write expressions for the linear accelerations at one IMU location in terms of those at the others. Using the right half of the RSDIMU as a reference and Eqs. (3) and (4) leads to the following results.

$$n_{x_L} = n_{x_R} + \delta n_x$$

$$= n_{x_R} + \delta n_{x_{\ell a_L}} - \delta n_{x_{\ell a_R}}$$

$$n_{y_L} = n_{y_R} + \delta n_y$$

$$= n_{y_R} + \delta n_{y_{\ell a_L}} - \delta n_{y_{\ell a_R}} + \delta n_{y_{B_L}} - \delta n_{y_{B_R}}$$
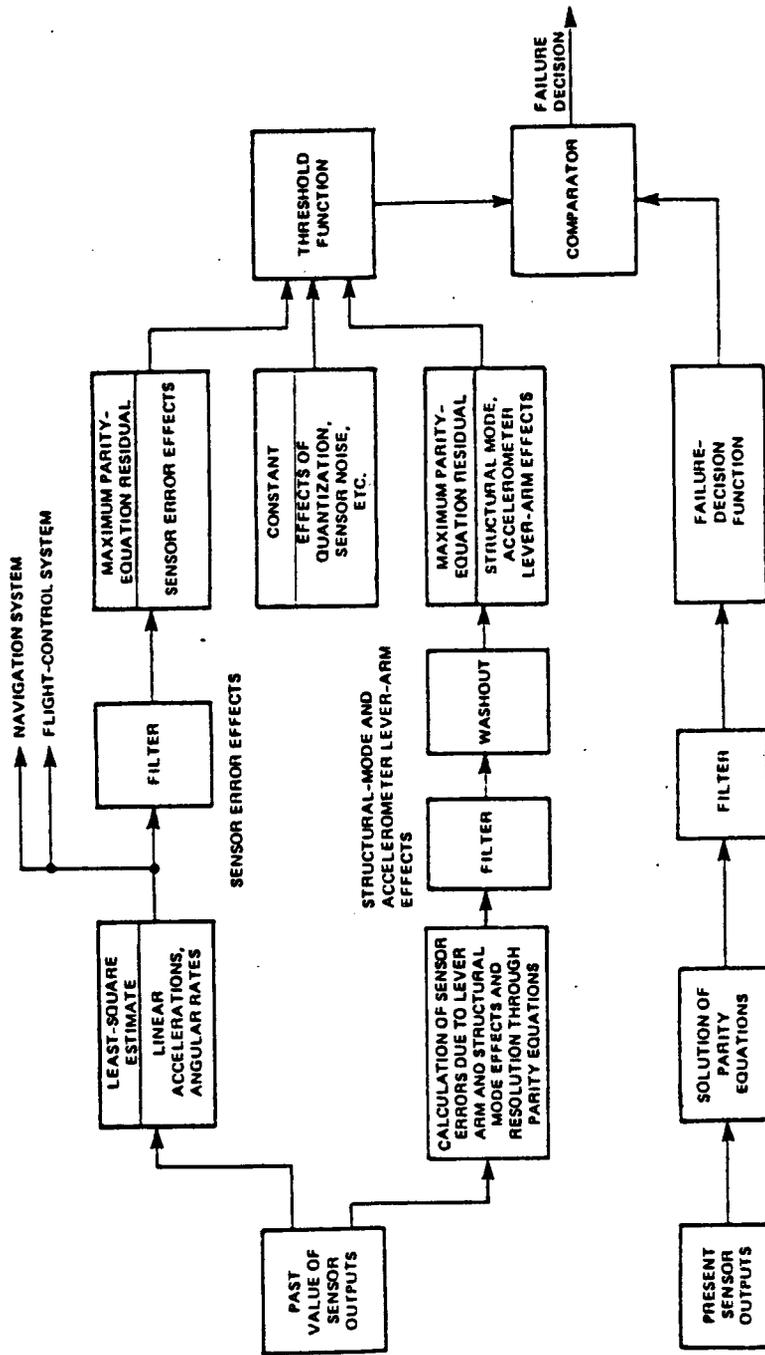
Figure 5. Block Diagram of Failure Detection Process —
Least Squares Estimation Approach

$$n_{z_L} = n_{z_R} + \delta n_z$$

$$= n_{z_R} + \delta n_{z_{\ell a_L}} - \delta n_{z_{\ell a_R}} + \delta n_{z_{B_L}} - \delta n_{z_{B_R}}$$

The output of the jth accelerometer of the right IMU can be written as

$$m_{a_j} = DT \cdot G_\phi \left\{ H_{j1} \cdot n_{x_R} + H_{j2} \cdot n_{y_R} + H_{j3} \cdot n_{z_R} + \delta m_{a_j} \right\}$$

$$j = A3, \ B3, \ A4, \ B4 \qquad (5)$$

δm_{a_j} is a term representing the sensor errors. The sensor models assumed for this study, described in detail in Reference 1, result in

$$\delta m_{a_j} = DT \cdot G_\phi \left\{ \lambda_j + (\mu_{j1} + \epsilon_j \cdot H_{j1}) n_{x_R} + (\mu_{j2} + \epsilon_j \cdot H_{j2}) n_{y_R} \right.$$

$$+ (\mu_{j3} + \epsilon_j \cdot H_{j3}) n_{z_R}$$

$$+ \alpha_{IP_j} (H_{j1} \cdot n_{x_R} + H_{j2} \cdot n_{y_R} + H_{j3} \cdot n_{z_R})$$

$$\cdot (H_{j1}^p \cdot n_{x_R} + H_{j2}^p \cdot n_{y_R} + H_{j3}^p \cdot n_{z_R})$$

$$\left. + \beta_{II_j} (H_{j1} \cdot n_{x_R} + H_{j2} \cdot n_{y_R} + H_{j3} \cdot n_{z_R})^2 \right\}$$

$$j = A3, \ B3, \ A4, \ B4 \qquad (6)$$

A similar expression is obtained for the output of the kth accelerometer of the left IMU using the appropriate accelerations. Use of the equations for the accelerations measured by the left half of the RSDIMU in terms of those of the right half leads to

$$m_{a_k} = DT \cdot G_\phi \left\{ H_{k1} \cdot n_{x_R} + H_{k2} \cdot n_{y_R} + H_{k3} \cdot n_{z_R} \right.$$

$$\left. + \delta m_{a_k} + H_{k1} \cdot \delta n_x + H_{k2} \cdot \delta n_y + H_{k3} \cdot \delta n_z \right\}$$

$$k = A1, \ B1, \ A2, \ B2 \qquad (7)$$

Substituting Eq. (5) and (7) into the parity equations results in the following residuals

$$\rho_i = \sum_j V_{ij} \, \delta m_{a_j} + \sum_k V_{ik} (H_{k1} \delta n_x + H_{k2} \delta n_y + H_{k3} \delta n_z) \ DT \cdot G_\phi$$

$$i = 1, 2, \ldots, n-3; \quad j = A1, B1, \ldots, A4, B4; \quad k = A1, B1, A2, B2 \qquad (8)$$

This expression results since VH = 0. It consists of two terms. The first results from the sensor errors and the second from the incremental structural mode and lever-arm effects between the locations of the two halves of the RSDIMU.

An upper bound for Eq. (8) is

$$\rho_{i_m} = \left(\sum_j |V_{ij}| \right) \delta m_{a_m} + \left| \sum_k V_{ik} (H_{k1} \delta n_x + H_{k2} \delta n_y + H_{k3} \delta n_z) \right| DT \cdot G_\phi$$

$$i = 1, 2, \ldots, n-3; \quad j = A1, B1, \ldots, A4, B4; \quad k = A1, B1, A2, B2 \qquad (9)$$

The dynamic threshold is then obtained by summing the squares of the upper bound for each parity equation, i.e., duplicating the generation of the decision function. The resulting expression is

$$T = \sum_{i=1}^{n-3} (\rho_{i_m})^2 \qquad (10)$$

In order to calculate the FDI system thresholds, Eq. (10), and hence Eq. (9), must be calculated in real time. Consider the first term

of Eq. (9). The V_{ij}'s are known and δm_{a_m} is an analytic expression for the upper bound of the sensor error effects given by

$$\delta m_{a_m} = DT \cdot G_\phi \left\{ \lambda_{a_m} + \mu_{a_m} \left(\left| n_{x_f} \right| + \left| n_{y_f} \right| + \left| n_{z_f} \right| \right) \right.$$

$$+ \varepsilon_{a_m} \left(\left| 0.788675 n_{x_f} \right| + \left| 0.788675 n_{y_f} \right| + \left| 0.577350 n_{z_f} \right| \right)$$

$$\left. + \left(\beta_{II_m} + \alpha_{IP_m} \right) \left[\left(\left| 0.788675 n_x \right| + \left| 0.788675 n_y \right| + \left| 0.577350 n_z \right| \right)^2 \right]_f \right\}$$

$$(11)$$

δm_{a_m} is obtained from Eq. (6) by assuming worst case conditions. For example, the magnitude of H_{j1}, H_{j2}, H_{j1}^P and H_{j2}^P is less than or equal to 0.788675, and the sensor errors are additive and bounded by their 3σ values.

Each term of Eq. (9) also contains a term which reflects the incremental value of the separation effects between the two IMU locations. If three or more independent measurements are available at each IMU location, the required quantities can be obtained by generating a least-squares solution for n_x, n_y, and n_z at each IMU location and differencing like quantities. This approach falls apart after the first failure is detected and isolated since one instrument is analytically removed from the system. Therefore, a least-squares solution can be obtained for only one IMU.

Reference 2 presents a technique for generating the incremental separation effects which overcomes the deficiencies of the approach described in the previous paragraph. The least-squares solution of only one of the IMUs is required. Assume for the purposes of discussion that the right IMU is selected as the reference. A least-squares solution can be obtained for the right IMU resulting in the estimated quantities $\hat{n}_{x_R}$, $\hat{n}_{y_R}$, and $\hat{n}_{z_R}$. An estimate of the separation effects on the instruments of the left IMU can be obtained by using $\hat{n}_{x_R}$, $\hat{n}_{y_R}$, and $\hat{n}_{z_R}$ to generate an

23

estimate of the measurements of the left IMU and subtracting them from the actual measurements. For example,

$$\hat{m}_{a_{A1}} = DT \cdot G_\phi \left\{ \alpha \hat{n}_{x_R} - \beta \hat{n}_{y_R} + \gamma \hat{n}_{z_R} \right\}$$

$$\delta \hat{m}_{a_{A1}} = m_{a_{A1}} - \hat{m}_{a_{A1}}$$

$$= DT \cdot G_\phi \left\{ \alpha (n_{x_L} - \hat{n}_{x_R}) - \beta (n_{y_L} - \hat{n}_{y_R}) + \gamma (n_{z_L} - \hat{n}_{z_R}) \right\}$$

$$= DT \cdot G_\phi \left\{ \alpha \delta \hat{n}_x - \beta \delta \hat{n}_y + \gamma \delta \hat{n}_z \right\} \qquad (12)$$

Following this procedure leads to

$$\delta \hat{m}_{a_{B1}} = DT \cdot G_\phi \left\{ -\beta \delta \hat{n}_x + \alpha \delta \hat{n}_y + \gamma \delta \hat{n}_z \right\}$$

$$\delta \hat{m}_{a_{A2}} = DT \cdot G_\phi \left\{ \beta \delta \hat{n}_x + \alpha \delta \hat{n}_y + \gamma \delta \hat{n}_z \right\}$$

$$\delta \hat{m}_{a_{B2}} = DT \cdot G_\phi \left\{ -\alpha \delta \hat{n}_x - \beta \delta \hat{n}_y + \gamma \delta \hat{n}_z \right\} \qquad (13)$$

Since the right IMU is the reference

$$\delta \hat{m}_{a_{A3}} = 0$$

$$\delta \hat{m}_{a_{B3}} = 0$$

$$\delta \hat{m}_{a_{A4}} = 0$$

$$\delta \hat{m}_{a_{B4}} = 0 \qquad (14)$$

The quantities needed for the thresholds are obtained by resolving the uncertainties of Eqs. (12), (13) and (14) through the parity equations, that is, solving the parity equations using these quantities for the sensor measurements. The absolute value of the solution is then used for the threshold.

Several additional items regarding the thresholds should be pointed out at this time. One is that the last value of the linear accelerations (generated for the flight-control system from the sensor signals) can be used to generate the thresholds. Using these signals results in thresholds which reflect the current state of the aircraft and its environment. In order to make a valid comparison between the residuals and thresholds, it is necessary to filter each in an identical fashion. It is preferable to filter the quantities required for the thresholds before the maximization and absolute values are generated. This results in a reduced level of noise which is not subject to maximization and leads to lower, more realistic thresholds. The subscript f in Eq. (11) indicates where the filtering of δm_{a_m} should occur in the generation of the thresholds.

The effect of failures on the thresholds has also been considered. The statistics of the parity equation residuals change to reflect the presence of a failure, e.g., the mean changes due to a bias failure. The thresholds will also change due to the failure, and detection and isolation is not possible. Modifications must be made to the FDI algorithm to eliminate this deficiency. The technique employed is to pass the estimated separation effects through washout filters before taking the absolute value for the thresholds. Washout filtering removes the effect of the instrument biases and bias failures from the separation effects so that the thresholds return to their prefailure values. The parity equation residuals change to reflect the effect of the failures and failure detection and isolation occurs when the thresholds are exceeded.

SECTION 3

A COMPARISON OF THE COMPENSATED AND UNCOMPENSATED GLT DECISION FUNCTIONS

3.1 Introduction

Previous investigations of the RSDIMU (References 1 and 2) have been concerned with the uncompensated GLT algorithm. That is, the decision functions of Eq. (1) and (2) have been used with the covariance matrix $C_\rho = I$. Simpler decision functions resulted. However, dynamic threshold compensation had to be employed to account for the aircraft system's environment, the sensor errors and the structural mode and accelerometer lever arm effects.

This section compares the uncompensated and compensated GLT decision functions. The motivation for investigating the compensated decision function is that it may be possible to employ constant thresholds if the sensed error effects are compensated for in the decision function. A simpler system with improved FDI performance may be possible.

A derivation of an analytic expression for the covariance matrix C_ρ, required for decision function compensation, is presented. This algorithm was implemented in the CSDL digital aircraft simulation and its FDI capability evaluated. Conclusions regarding the feasibility of this approach, its pros and cons and a comparison with results obtained for the uncompensated GLT decision function are presented. Colocated sensors are assumed for the initial evaluation, thereby simplifying the evaluation of the concept since the structural mode and accelerometer effects can be neglected. Reference 3 provided the basis for this study.

3.2 Derivation of the Error Covariance Matrix

In the presence of instrument errors, the instrument outputs can be represented by

$$m = H\omega + \underline{e}_1 + \underline{e}_2 + \ldots \underline{e}_k$$

Thus, the parity vector can be written as

$$\rho = Vm = V\underline{e}_1 + V\underline{e}_2 + \ldots V\underline{e}_k$$

$$= \underline{\varepsilon}_1 + \underline{\varepsilon}_2 + \ldots \underline{\varepsilon}_k$$

Assuming that the error sources $\underline{e}_i$ are uncorrelated, the covariance of ρ, C_ρ is given by

$$C_\rho = C_1 + C_2 + \ldots C_k$$

where

$$C_i = E\left[\underline{\varepsilon}_i \underline{\varepsilon}_i^T\right] = VE\left[\underline{e}_i \underline{e}_i^T\right]V^T$$

$$= VR_i V^T$$

and R_i is the covariance of $\underline{e}_i$.

The error sources for the two-degree-of-freedom instruments considered are:

$\underline{e}_1$ = error due to instrument biases

$\underline{e}_2$ = error due to scale factor errors and input axis misalignments

$\underline{e}_3$ = error due to g-sensitivities of the input axes (g-sensitive bias)

$\underline{e}_4$ = quantization and sensor noise

The covariance of the error term due to instrument biases and hysteresis is given by

$$R_1 = \begin{bmatrix} \sigma_1^2 & \rho_c & & & & \\ & & & 0 & & 0 \\ \rho_c & \sigma_1^2 & & & & \\ \hline & & & \ddots & & \\ & 0 & & & & 0 \\ \hline & & & & & \\ & & & & \sigma_1^2 & \rho_c \\ & 0 & & 0 & & \\ & & & & \rho_c & \sigma_1^2 \end{bmatrix}$$

where

- σ_1^2 is the sum of the squares of the 1-sigma values of the instrument bias, hysteresis, etc.

- ρ_c is the correlation coefficient between the instrument pair.

The covariance matrix R_1 is of dimension [n×n].

The error term $\underline{e}_2$ is given by

$$\underline{e}_2 = H_m \omega$$

where the elements of H_m represent the instrument scale factor errors and input axis misalignments. The contribution of this term to the total parity vector is given by

$$\underline{\epsilon}_2 \;=\; VH_m\omega$$

$$=\; \overline{A}\omega$$

$\underline{\epsilon}_2$ can also be expressed as

$$\underline{\epsilon}_2 \;=\; \hat{\Omega}\underline{a}$$

where

$$\hat{\Omega} \;=\; \begin{bmatrix} \hat{\omega}^T & | & 0\;0\;0 & | & 0\;0\;0 & | & \\ \hline 0\;0\;0 & | & \hat{\omega}^T & | & & | & \\ \hline & | & & | & \hat{\omega}^T & | & \\ & | & & | & & \cdot\;\cdot\;\cdot & \\ \hline \cdot & | & & | & 0\;0\;0 & | & \hat{\omega}^T \end{bmatrix}$$

and

$$\underline{a} \;=\; (\overline{A}_{11}\overline{A}_{12}\overline{A}_{13}\overline{A}_{21}\overline{A}_{22}\overline{A}_{23}\cdots\overline{A}_{m1}\overline{A}_{m2}\overline{A}_{m3})^T$$

where $\hat{\omega}$ is the most recent estimate of ω

$$\hat{\omega} \;=\; (H^TH)^{-1}H^Tm$$

Therefore, C_2 is calculated as

$$C_2 \;=\; \hat{\Omega}\,R_{\underline{a}}\,\hat{\Omega}^T$$

30

The derivation of R_a includes the cross correlation between the instrument pairs.

$\underline{a}$ can also be expressed as

$$\underline{a} = V^* \underline{h}_m$$

where

$$V^* = \begin{bmatrix} V_{11}I_3 & V_{12}I_3 \cdots\cdots\cdots\cdots\cdots V_{1n}I_3 \\ V_{21}I_3 \cdots\cdots\cdots\cdots\cdots\cdots\cdots\cdots\cdots V_{2n}I_3 \\ V_{n-3,1}I_3 \cdots\cdots\cdots\cdots\cdots\cdots\cdots\cdots V_{n-3,n}I_3 \end{bmatrix}$$

and

$$\underline{h}_m = \begin{bmatrix} H_{m_{11}} & H_{m_{12}} & H_{m_{13}} & H_{m_{21}} & \cdots\cdots & H_{m_{n3}} \end{bmatrix}^T$$

The covariance of $\underline{a}$ is given by

$$R_a = E[\underline{a}\,\underline{a}^T] = E[V^* \underline{h}_m \underline{h}_m^T V^{*T}]$$

$$= V^* R_m V^{*T}$$

where

$$R_m = E[\underline{h}_m \underline{h}_m^T]$$

31

The vector $\underline{h}_m$ may be partitioned as follows:

$$\underline{h}_m^T = [\underline{h}_{m_1}^T \quad \underline{h}_{m_2}^T \quad \cdots \quad \underline{h}_{m_n}^T]$$

where $\underline{h}_{m_i}^T$ is the i-th row of H_m. Since the instrument errors between each instrument axis pair are dependent

$$R_m = \begin{bmatrix} R_{m_{11}} & R_{m_{12}} & 0_{3x3} & 0_{3x3} & & \\ R_{m_{21}} & R_{m_{22}} & 0_{3x3} & 0_{3x3} & & \\ & & R_{m_{33}} & R_{34} & & \\ & & R_{m_{43}} & R_{m_{44}} & & \\ & & & & \ddots & \\ & & & & R_{m_{n-1,n-1}} & R_{m_{n-1,n}} \\ & & & & R_{m_{n,n-1}} & R_{m_{nn}} \end{bmatrix}$$

where

$$R_{m_{ij}} = E[\underline{h}_{m_i} \underline{h}_{m_j}^T]$$

R_m has dimension $[3n \times 3n]$.

$\underline{R}_a$ can be written as (see Reference 3)

$$\underline{R}_a = \sigma_{MIS}^2 I_{3(n-1)x3(n-1)} + (\sigma_{SF}^2 - \sigma_{MIS}^2) V^* R_m V^{*T}$$

Thus, C_2 is given by

$$C_2 = \hat{\Omega}[\sigma^2_{MIS} I_{3(n-1)x3(n-1)} + (\sigma^2_{SF} - \sigma^2_{MIS})V^* R_m V^{*T}]\hat{\Omega}^T$$

The ith element of the error term due to the g-sensitivity of the input axes, $\underline{e}_{3i}$, is given by

$$\underline{e}_{3i} = n_z H_{i3} S_{gi}$$

It is assumed that the normal acceleration is much greater than the longitudinal and lateral accelerations.

Thus, R_3 can be written

$$R_3 = E[\underline{e}_3\underline{e}_3^T]$$

$$= n_z^2\sigma^2_{S_g} \begin{bmatrix} H^2_{13} & & & & \\ & H^2_{23} & & & \\ & & \cdot & & \\ & & & \cdot & \\ & & & & \cdot \\ & & & & & H^2_{n3} \end{bmatrix}$$

Therefore,

$$C_3 = (n_z\sigma_{S_g})^2 V \begin{bmatrix} H^2_{13} & & \\ & \cdot \cdot & \\ & & \cdot \\ & & & H^2_{n3} \end{bmatrix} V^T$$

33

Sensor noise is not considered in this phase of the study. The quantization compensation parameter is obtained from a straight and level flight simulation in the absence of sensor noise and error. A compensation magnitude which corresponds to a bias error of 0.03 deg/hr has been used nominally.

To summarize, the error-compensated detection decision function can be described as

$$DF_{DC} = \rho^T[V(R_1 + R_2 + R_3 + R_4)V^T]^{-1}\rho$$

$$= \rho^T[C_1 + C_2 + C_3 + C_4]^{-1}\rho$$

$$= \rho^T C_\rho^{-1}\rho$$

At each measurement sampling period, C_ρ is updated and the compensated decision function compared to a threshold to determine whether a failure has occurred. When a failure is detected, it is isolated to the sensor which maximizes the compensated isolation decision function given by Equation (2).

3.3   Results

Simulation results were obtained for the purpose of comparing the uncompensated and compensated decision functions for failure detection purposes. Two forms of the compensated failure detection decision were actually compared; the complete one as derived in the previous section and a simplified one determined using only the diagonal elements of C_ρ in the compensation. This, of course, simplifies the calculation of C_ρ^{-1}.

Figure 6 shows the compensated and uncompensated failure decision functions obtained for the nominal sensor error parameters. The effect of the compensation is reflected in the difference in magnitude between

34

the two types of decision functions. Furthermore, it is apparent that
the compensation is not perfect as evidenced by the peaks in the compen-
sated decision function which occur when the vehicle maneuvers. This
means that the sensor error effects will have to be accurately identified
to achieve a decision function which is not affected by the vehicle
dynamics so that constant thresholds can be implemented. Otherwise the
risk of a high false alarm rate exists. The results of Figure 6 also
indicate that the simplified compensated decision function may be used in
lieu of the unsimplified one since their time histories are generally the
same, differing only in magnitude.

To allow a more thorough investigation of the compensated GLT
decision function, the nominal error parameters used in the calculation
of C_ρ were adjusted to reflect the variance of the actual sensor error
parameters in the simulation. The scale factor and misalignment errors
used to calculate C_ρ were increased by a factor of 5 and the g-
sensitive errors by 24. Under this assumption, the peak value of the
unsimplified compensated decision function was reduced by a factor of 6
and the simplified one by a factor of 16. Fairly uniform decision
functions resulted.

Bias failures were introduced during the 30 minute simulation run
according to the time history given in Table 4. In this table, as in
others which follow, sensor axes 1, 3, 5 and 7 correspond to axis A of
instruments 1, 2, 3 and 4, respectively, while sensor axes 2, 4, 6 and 8
correspond to axis B of the same instruments. The performance of the
uncompensated and compensated GLT detection decision functions is shown
in Figures 7, 8 and 9 for the adjusted sensor error parameter case. The
results indicate that the compensated decision functions are quite
sensitive to a failure during a relatively mild maneuver. However, the
effect of the failure is not present in the decision function during
large roll maneuvers. This is due to the effect of the dynamic compensa-
tion term C_2. No significant difference in performance can be observed
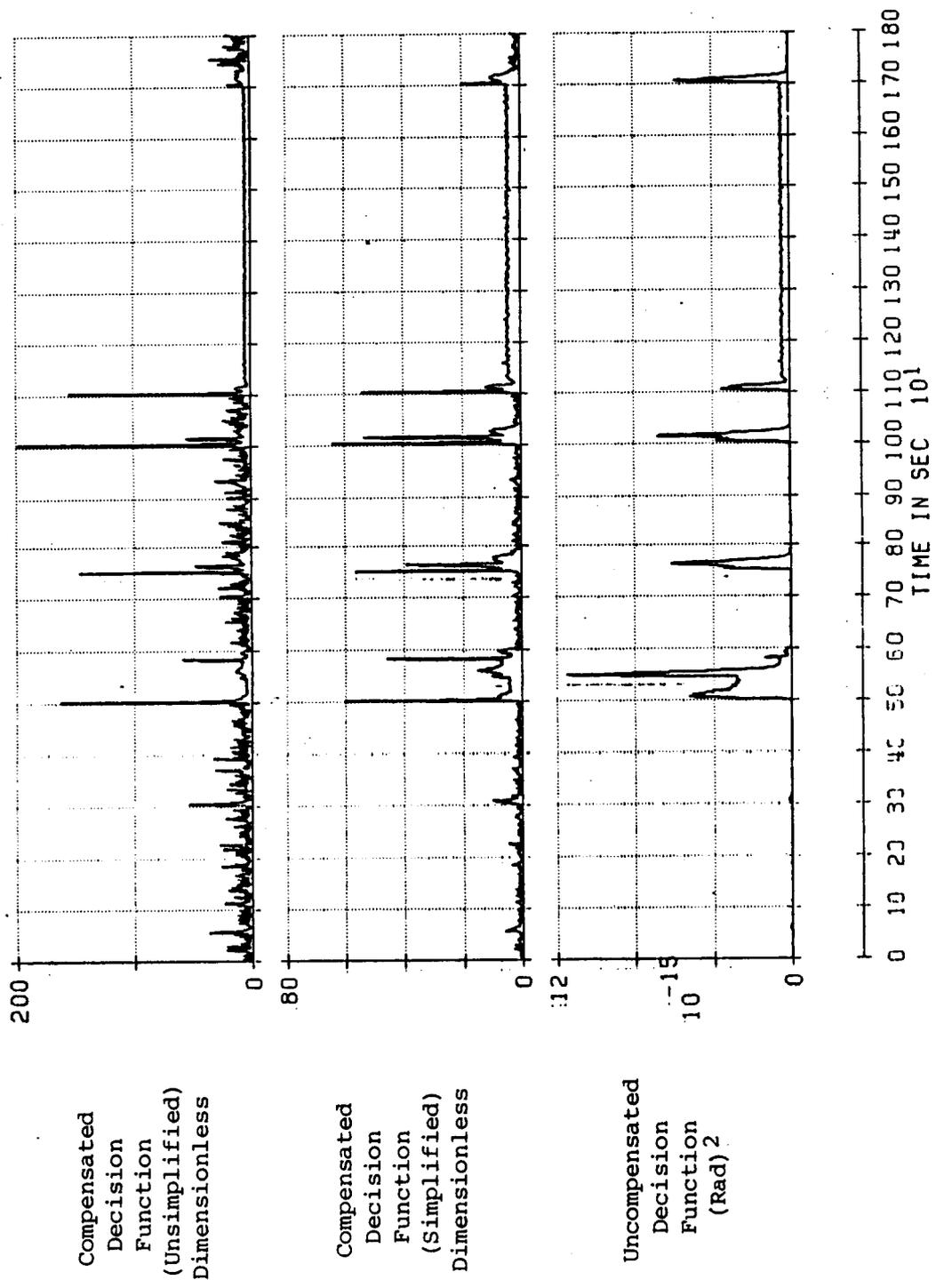between the simplified and unsimplified compensated detection decision

Figure 6. Compensated and Uncompensated GLT Detection Decision Functions, No Failures Present, Nominal Sensor Error Statistics, 30 Minute Evaluation Trajectory

36

Table 4
Failure Profile for the 30 Minute Evaluation Trajectory

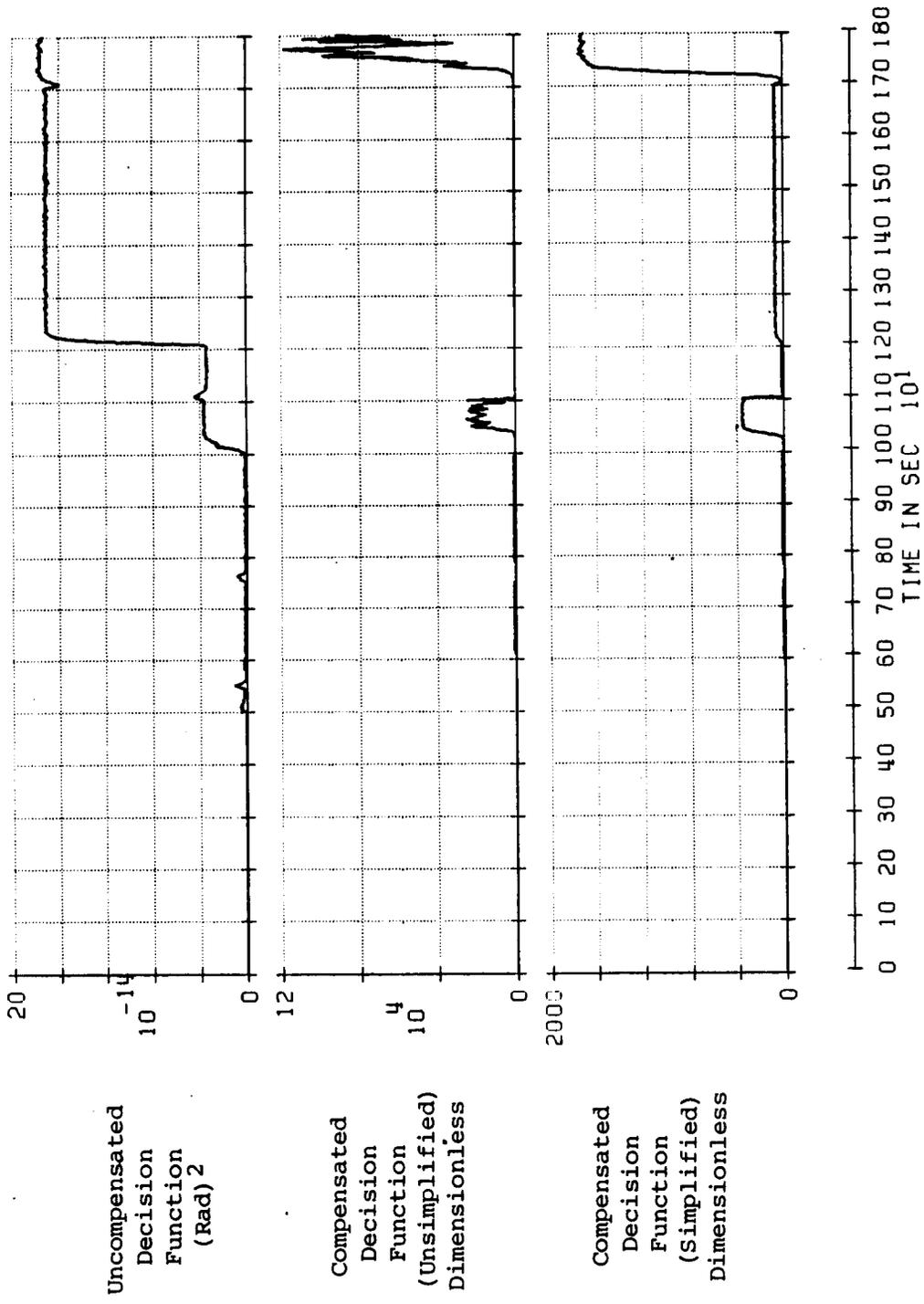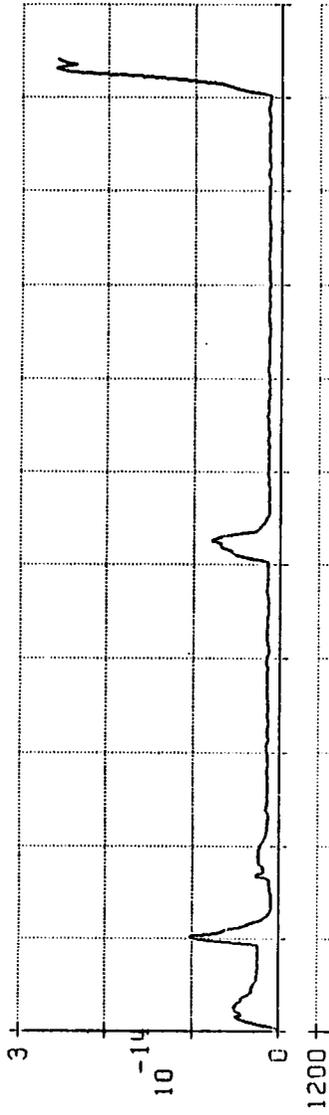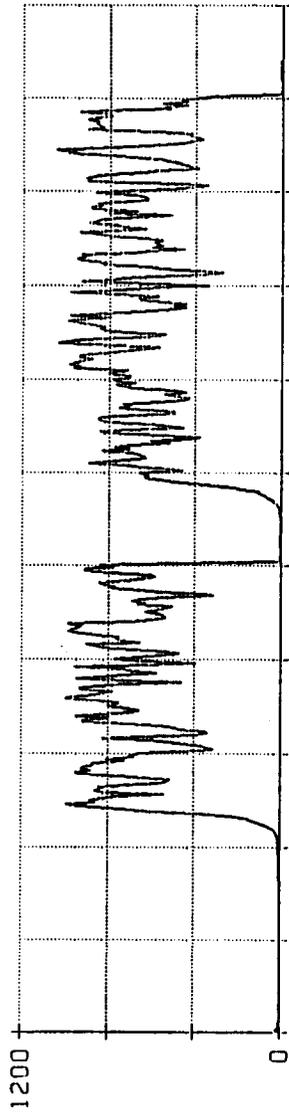| TIME (sec)	FAILURE MAGNITUDE (deg/hr)	SENSOR AXIS FAILED
505	0.5	4
1005	2.0	4
1205	3.0	4

Figure 7. Compensated and Uncompensated GLT Detection Decision Functions with Failures Present, Adjusted for Sensor Error Statistics, 30 Minute Evaluation Trajectory

Figure 8. Compensated and Uncompensated GLT Detection Decision Functions with Failures Present, Adjusted for Sensor Error Statistics, 500-1050 Sec of 30 Minute Evaluation Trajectory

39
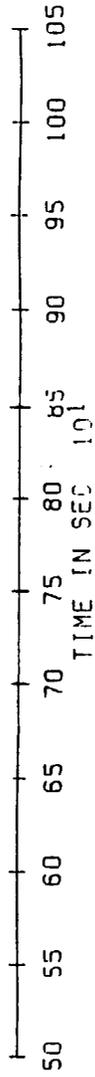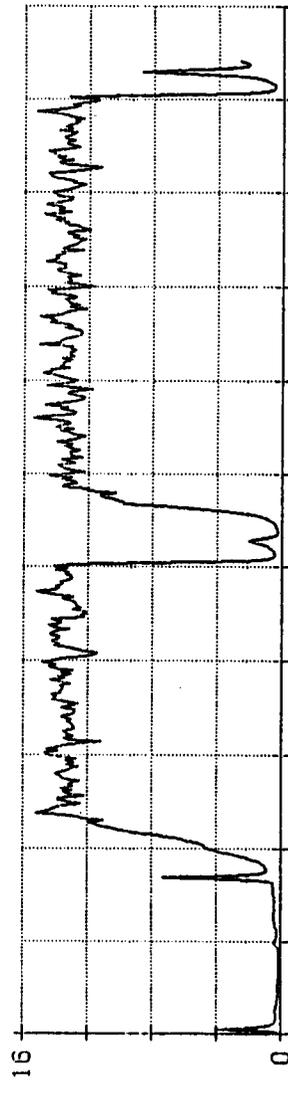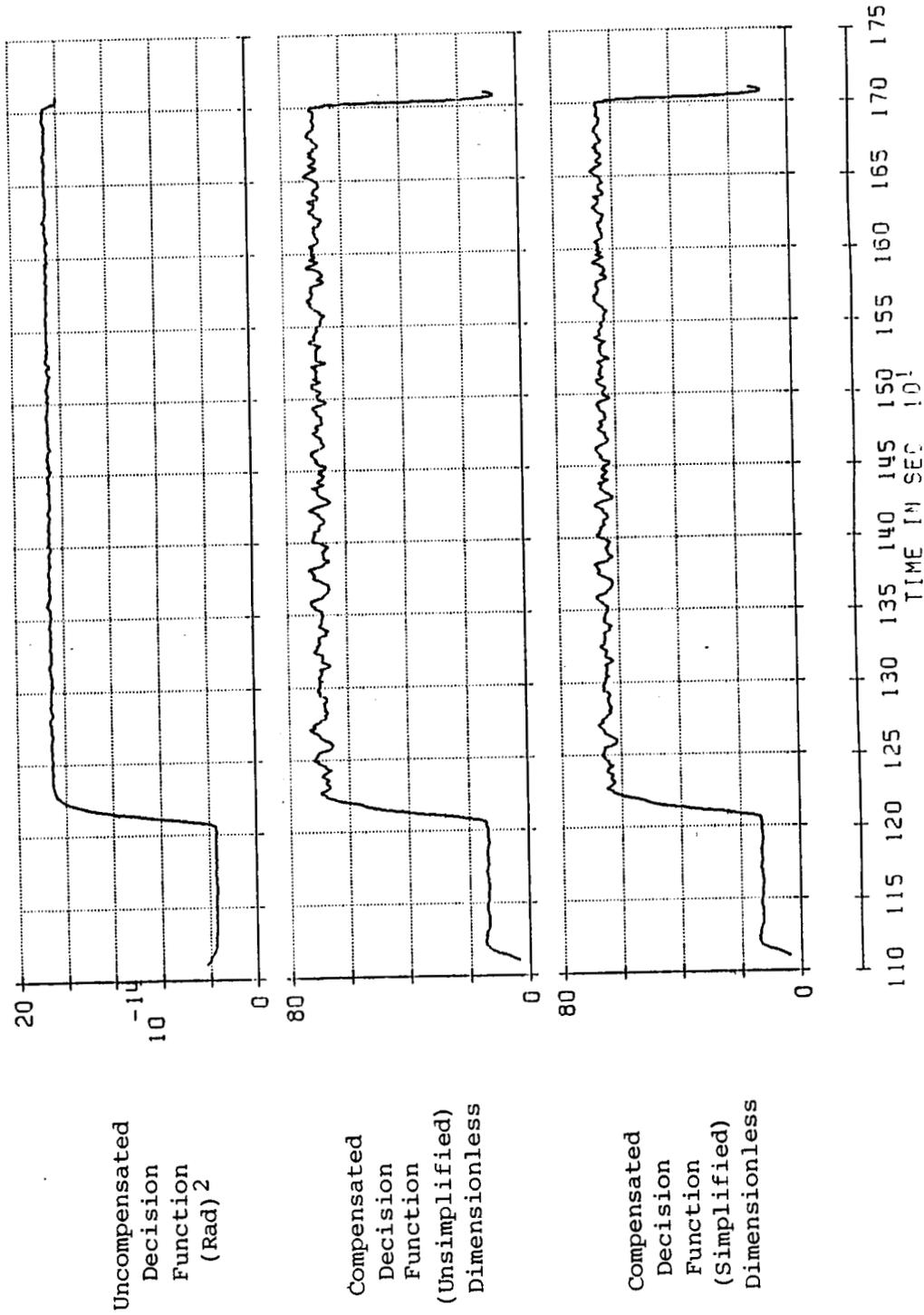
Figure 9. Compensated and Uncompensated GLT Detection Decision Function with Failures Present, Adjusted for Sensor Error Statistics, 1100-1750 Sec of 30 Minute Evaluation Trajectory

40

functions. It is also apparent that the effect of the failure is not as clearly evident in the uncompensated decision function as in the compensated ones.

To gain more insight into the performance of the compensated detection decision functions during large maneuvers the shorter 110 second flight profile defined in Table 3 was considered. Results are shown in Figure 10 for the adjusted sensor parameter case with no failures. The corresponding results in the presence of failures are shown in Figure 11. The failure profile is presented in Table 5. The failure effect is clearly evident when the flight is level and unaccelerated (0-40 sec). The sensitivity of the compensated detection decision function to the failure decreases during the maneuver. It appears that the failure can be detected with the simplified compensated detection decision function during the maneuver even though its magnitude has decreased at the start of the maneuver. Failure detection does not appear possible with the uncompensated detection decision function in this specific case.

3.4 Conclusions

The following conclusions can be drawn from this phase of the study.

- The results obtained for the GLT FDI approach which compensates for the effects of sensor errors on the detection decision function looks encouraging. The study provided better insight into the failure detection process.

- In all the cases considered, the use of only the diagonal elements in the computation of the detection decision function yielded very favorable results. This reduces the computational burden of inverting the updated matrix C_ρ.

- The compensated detection decision function shows remarkable sensitivity to small bias failures during level and unaccel-

41
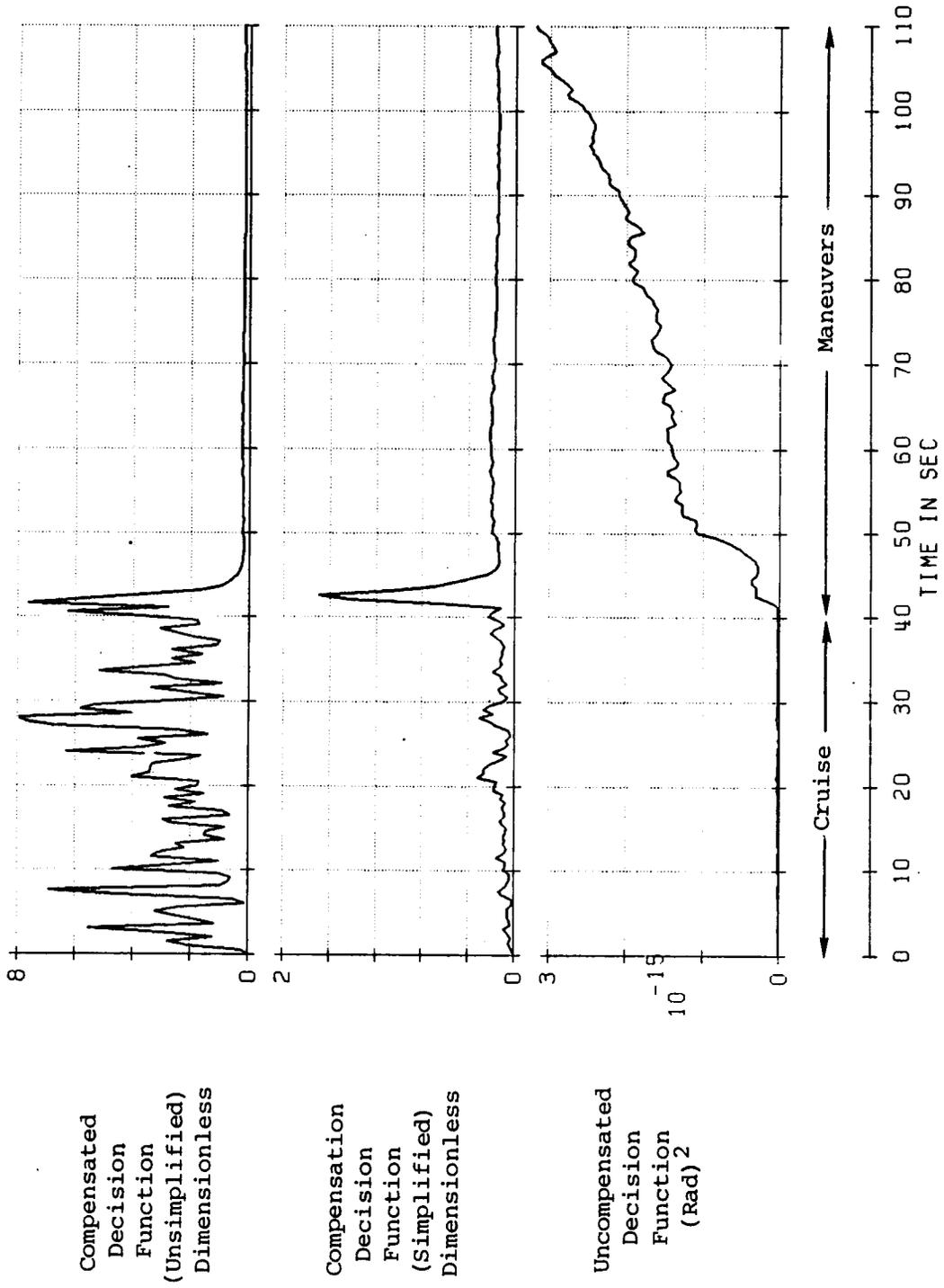
Figure 10. Compensated and Uncompensated GLT Detection Decision Functions with No Failures Present, Adjusted for Sensor Error Statistics, 110 Second Evaluation Trajectory

42
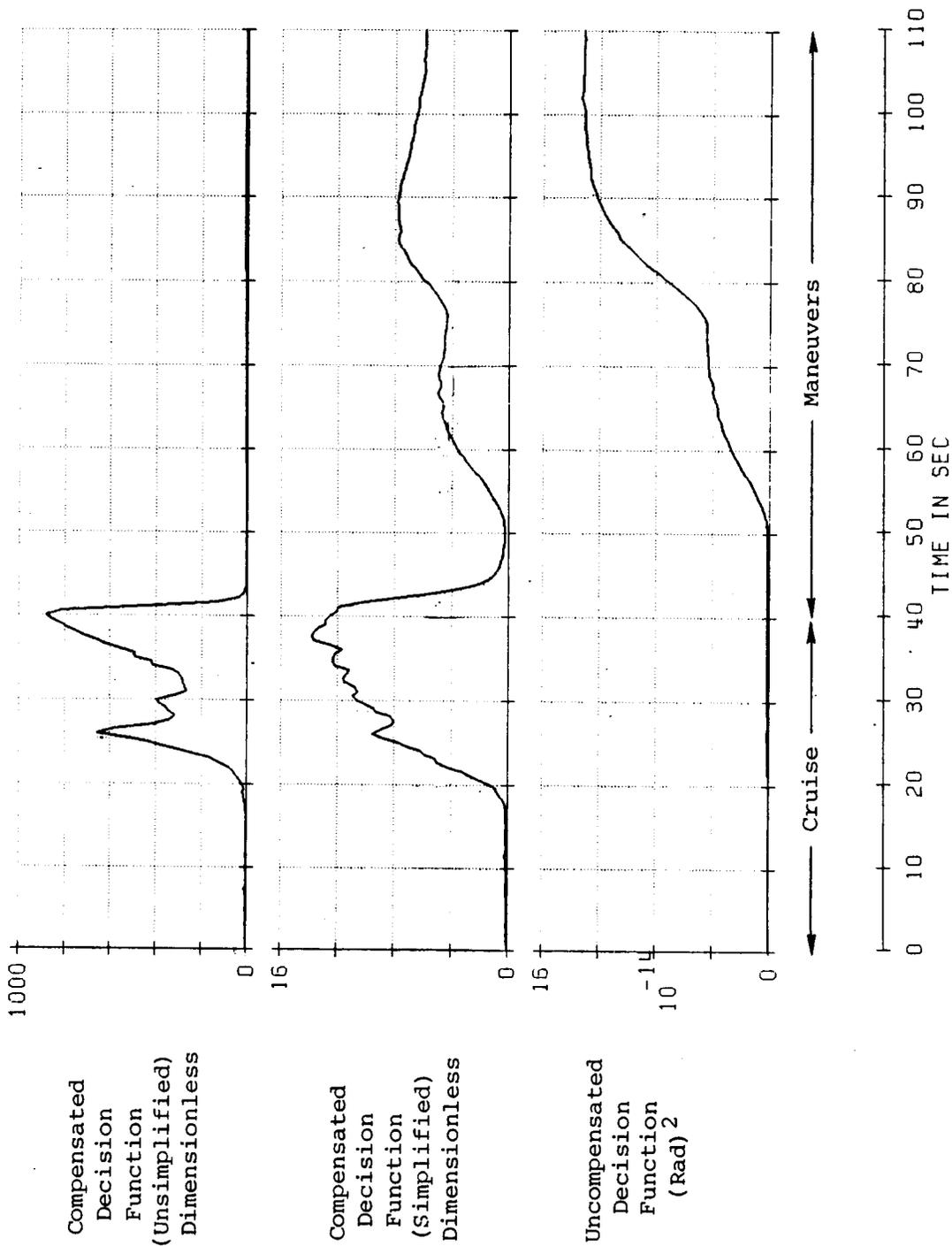
Figure 11. Compensated and Uncompensated GLT Detection Decision Functions with Failures Present, Adjusted for Sensor Error Statistics, 110 Second Evaluation Trajectory

43

Table 5

Failure Profile for the 110 Second Evaluation Trajectory

TIME (sec)	FAILURE MAGNITUDE (deg/hr)	SENSOR AXIS FAILED
15	0.5	4
50	2.5	4
75	3.0	4

erated flight and mild maneuvers. However, the problem of detecting failures during maneuvers is still unresolved.

- It is still premature to consider this FDI scheme as a potential alternative to dynamic threshold compensation. This approach, however, deserves additional attention.

SECTION 4

NOISE COMPENSATION FOR FDI SYSTEMS

The effects of sensor noise on the performance of the FDI system are investigated. This subject has received little attention thus far. The need for noise compensation in the dynamic thresholds is established and a method for accomplishing this is derived based upon the compensated detection decision function approach of the previous section. The magnitude of the noise level, the degree of noise compensation, i.e., whether to compensate 1σ or 2σ, etc., and the detection filter time constants are all considered in this phase of the study. The effects of sensor failures are also examined.

4.1 Derivation of the Sensor Noise Compensation Algorithm

The sensor noise is compensated for in the threshold by using the estimated noise variance. The parity equation residuals, the nominal sensor parameters, and the estimated lever arm and structural mode effects are used to estimate the noise variance.

In the absence of failure, the parity equation residual is given by

$$\rho = Vm = \varepsilon_{SE} + \varepsilon_{NOISE} + \varepsilon_{SM}$$

where

47

ε_{-SE} = sensor error residuals

ε_{-NOISE} = sensor noise residuals excluding structural mode and lever arm

ε_{-SM} = residuals due to structural mode and lever arm effect.

The variance of the parity equation residuals is given by

$$\sigma_p^2 = E\left[(\rho)^2\right] \simeq E[\varepsilon_{-SE}^2] + E[\varepsilon_{-NOISE}^2] + E[\varepsilon_{-SM}^2]$$

It is assumed that the three error sources are independent. The noise variance can be expressed as

$$\sigma_{\varepsilon_{-NOISE}}^2 = \sigma_\rho^2 - \sigma_{\varepsilon_{-SE}}^2 - \sigma_{\varepsilon_{-SM}}^2$$

The variance of the parity equation residuals can be computed dynamically from the time history of the parity equation. The sensor error contribution is computed using the covariance estimation approach developed in the previous section. The variance of the structural mode and accelerometer lever arm effects is determined by taking the expected value of the square of the acceleration due to these quantities.

4.2 Results

The sensor noise compensation was implemented in the gyro soft failure channel only. Compensation was not used in the accelerometer channel because results indicated that this portion of the FDI system was not very sensitive to the presence of noise. Four important parameters that affect the performance of the FDI system were considered. They are

- noise level,

- magnitude of the noise compensation,

48

- time constant of the soft failure detection channel,

- magnitude of the sensor failure.

A straight and level cruise flight profile was used in all of the simulation runs. The effects of sensor separation and structural modes are not included for simplicity.

The variance of the noise level is assumed to be constant for a given type of sensor. A value of 0.00284g was assumed for the accelerometers and 49.5 deg/hr for the gyros. The nominal level of the gyro noise compensation is 1σ. The soft failure detection channel second order filter time constant is varied from the nominal value of $\sqrt{15.0}$ seconds. A damping ratio of one is always assumed. Bias failures of various magnitudes have been considered. The failure profile is presented in Table 6 for the base case.

Table 7 indicates the need for noise compensation in the gyro detection channel. The noise level must be about 5.0 deg/hr or less to avoid false alarms without compensation. The accelerometer detection channel, on the other hand, is not very sensitive to noise. Hence, accelerometer noise compensation may not be necessary.

Table 8 summarizes the effect of the filter time constant on FDI system noise compensation. False alarms can be reduced by increasing the time constant of the filters. The accelerometer channel is not very sensitive to the filter time constant although there is a trend toward increasing detection time delay with increasing time constant. The results also indicate that the gyro channel time constants have to be large; about 100 seconds, without noise compensation. The use of large time constants alone to compensate for noise effects does not prevent the possibility of FDI system errors in the presence of sensor failures. The false isolation which occurred for the case where failures were introduced confirms this conclusion.

The effects of noise compensation, the filter time constant and sensor failures on FDI system performance are summarized in Table 9. In

Table 6
Failure Profile for Noise Compensation Study

Accelerometer
(Noise Level .00284 g)

TIME (sec)	MAGNITUDE (g)	FAILED SENSOR AXIS
60	0.003	4
130	0.003	6
200	0.003	8

Gyro
(Noise Level 49.5°/hr)

TIME (sec)	MAGNITUDE (deg/hr)	FAILED SENSOR AXIS
70	4.0	8
140	4.0	6
210	4.0	4

Table 7

Effect of Sensor Noise Level on FDI System Performance

ACCELEROMETER NOISE STANDARD DERIVATION (g)	GYRO NOISE STANDARD DEVIATION (deg/hr)	COMMENTS
0	0	No false alarm
.00284	49.5	False alarm in the gyro channel only
0	49.5	False alarm in the gyro channel
0	10.0	False alarm in the gyro channel
0	5.0	No false alarm
.00284	0	No false alarm
.0142	0	No false alarm
.0284	0	False alarm in the accelerometer channel

Table 8

Effect of Filter Time Constant on FDI System Performance,
Nominal Noise Level, No Noise Compensation

ACCELEROMETER FILTER TIME CONSTANT (sec)	GYRO FILTER TIME CONSTANT (sec)	ACCELEROMETER FAILURE MAGNITUDE (g)	GYRO FAILURE MAGNITUDE (deg/hr)	COMMENTS
√15	√15	0.	0.	Nominal Case False Alarm in Gyro Channel
15.	15.	0.	0.	False Alarm in Gyro Channel
60.	60.	0.	0.	False Alarm in Gyro Channel
100.	100.	0.	0.	No False Alarm
100.	100.	0.003	2.0	False Isolation in Gyro Channel

the absence of a failure, no false alarm occurred in the soft gyro detection channel with 1σ noise compensation. The gyro failure level that can be detected under these conditions is about 4.0 deg/hr. The correct detection of a 2.0 deg/hr gyro failure is very sensitive to the filter time constant as indicated by Cases 2, 4, 5 and 6. False alarms can be avoided by increasing the level of noise compensation as demonstrated by Cases 8 and 9.

Time histories of the soft failure channel thresholds and detection decision functions for two representative cases with sensor noise, with and without compensation, are presented in Figures 12 and 13, respectively. The soft failure channel filter time constant is $\sqrt{15}$ sec and the nominal noise level is 49.5 deg/hr. A white noise model, with a power spectrum which is constant over all frequencies, was assumed. This characteristic accounts for the fact that soft failure decision functions on the order of tenths of a deg/hr are evident in Figures 12 and 13 and demonstrates a potential problem with FDI for the RSDIMU. The white noise model introduces signals at frequencies within the passband of the soft failure channel low pass filter which are attenuated very little compared to the high frequency noise components and possibly not at all in the worst case.

Figure 12 was obtained for the system without noise compensation in the threshold. Three false alarms, due to the presence of the noise, were rapidly detected between 50 to 75 sec into the run, clearly demonstrating the need for compensation. The software was specifically written to exclude the detection of failures for the first 45 sec of a simulation run and is the reason that false alarms were not encountered prior to the times indicated on Figure 12. Furthermore, the software is also written so that the thresholds are not computed after three failures are detected and explains why the threshold is zero for times greater than 75 seconds.

The results of Figure 13 were obtained with 1σ noise compensation in the threshold and three 4 deg/hr failures introduced as indicated in

Table 9

Effect of Filter Time Constant, Failure Magnitude and
Noise Compensation Level on FDI System Performance

| CASE	ACCELEROMETER FILTER TIME CONSTANT (sec)	GYRO FILTER TIME CONSTANT (sec)	ACCELEROMETER FAILURE MAGNITUDE (g)	GYRO FAILURE MAGNITUDE (deg/hr)	NOISE COMPENSATION LEVEL	COMMENTS
1	$\sqrt{15.0}$	$\sqrt{15.0}$	0.	0.	1σ	No False Alarm
2	$\sqrt{15.0}$	$\sqrt{15.0}$	0.003	2.0	1σ	Gyro Failures Undetected
3	$\sqrt{15.0}$	$\sqrt{15.0}$	0.003	4.0	1σ	Gyro Failures Detected with Long Time Delay
4	20.0	20.0	0.003	2.0	1σ	False Isolation in the Gyro Channel
5	60.0	60.0	0.003	2.0	1σ	Accelerometer Failures Detected with Long Delay, False Isolation in Gyro Channel
6	90.0	90.0	0.003	2.0	1σ	Both Gyro and Accelerometer Failures Detected with Long Delays
7	$\sqrt{15.0}$	20.0	0.003	2.0	3σ	Gyro Failures Undetected
8	$\sqrt{15.0}$	10.0	0.003	4.0	3σ	Gyro Failures Undetected
9	$\sqrt{15.0}$	10.0	0.003	4.0	1.5σ	Third Gyro Failure Not Detected
10	$\sqrt{15.0}$	$\sqrt{15.0}$	0.003	6.0	1σ	Gyro Failures are Detected with Long Delays
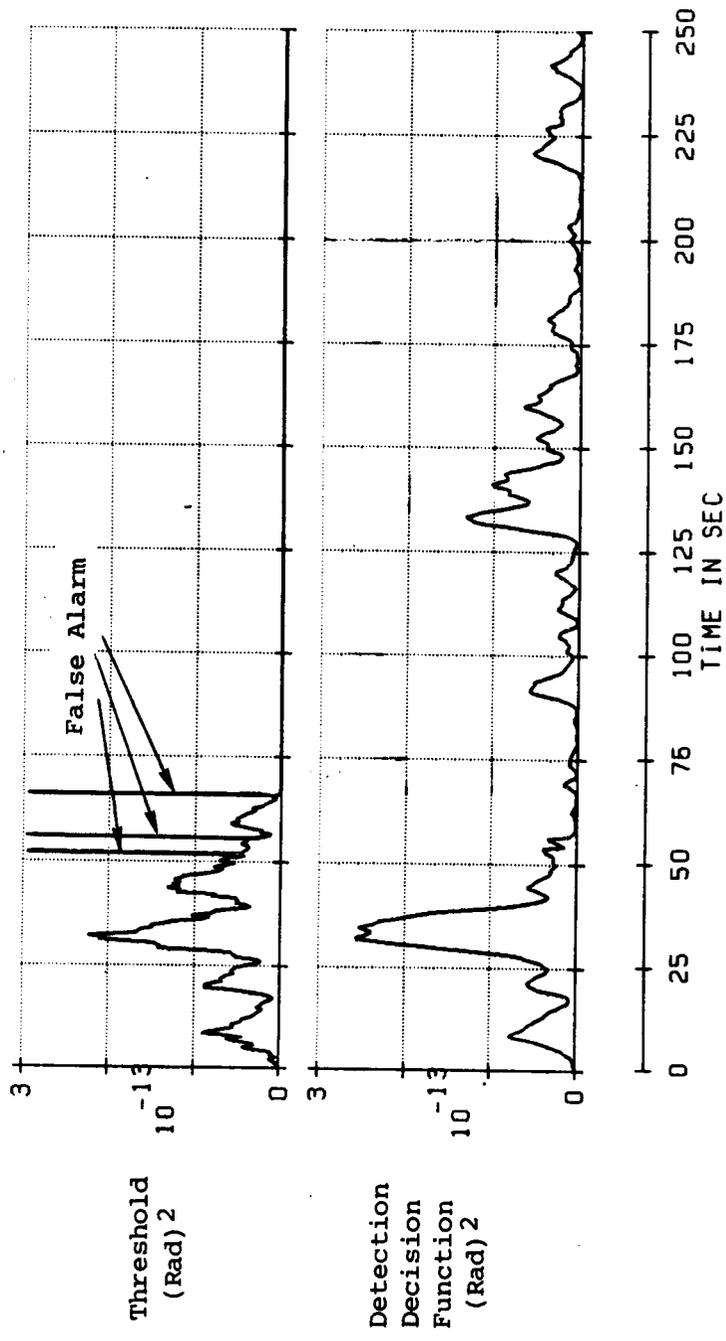
Figure 12. Gyro Soft Failure Channel Threshold and Detection Decision
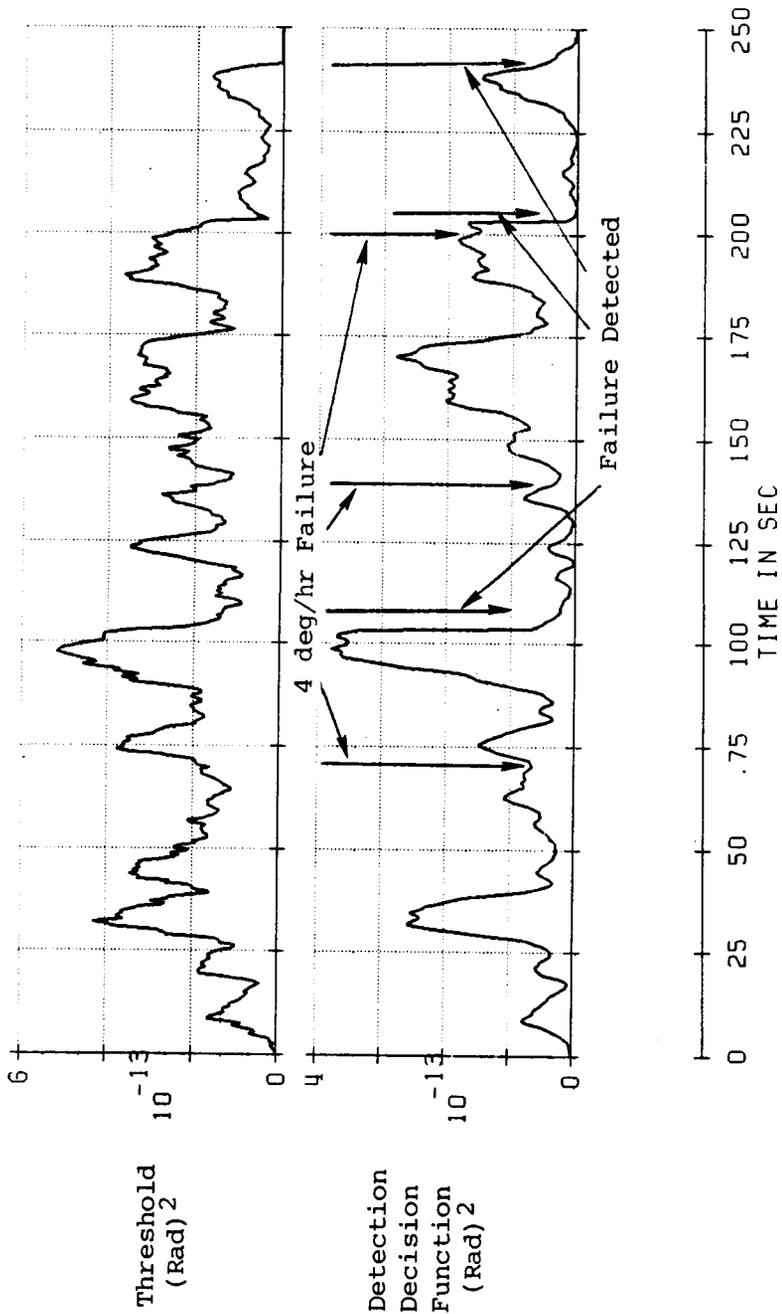Function, No Noise Compensation, Cruise Flight Condition

Figure 13. Gyro Soft Failure Channel Threshold and Detection Decision Function, Noise Compensation, Cruise Flight Condition

Table 6. The nominal sensor error values were used to compute the noise compensation and not the adjusted values which led to the results presented in Figure 11. The three failures were detected and correctly isolated. In fact, the second failure was detected after the third was introduced and its effect not fully manifested in the decision function. The results of Figure 13 confirm the validity of noise compensation in the failure detection system thresholds.

4.3   Summary and Conclusions

The performance of the FDI algorithm in the presence of noise has been investigated. The effects of noise level, failure level, noise compensation level and filter time constants have been considered. A straight and level flight profile has been used for simulation purposes.

Several conclusions were drawn during the course of this study. They were:

- Gyro noise compensation is necessary to prevent false alarms. Without noise compensation, the gyro detection channel can only tolerate a low noise level of about 5 deg/hr. However, the accelerometer channel is not very sensitive to noise.

- Noise can be compensated for by adjusting the filter time constants of the FDI system or by accounting for the presence of noise in the detection threshold using a covariance computation scheme.

- Large filter time constants by themselves are not sufficient to prevent false alarms in the presence of noise and failures. Noise compensation in the threshold is necessary.

- A high level of noise compensation in the threshold provides a means of preventing false alarms at the expense of decreased failure detection capability.

SECTION 5

THE EFFECT OF SENSOR LOCATION AND MAGNITUDE OF THE STRUCTURAL MODES ON FDI SYSTEM PERFORMANCE

5.1   Introduction

The impact of sensor location and magnitude of the structural mode effects on FDI system performance must be considered in the implementation and utilization of an RSDIMU in an aircraft system. Given complete freedom, the aircraft control system designer will place the accelerometers at the nodes and the gyros at the antinodes of the structural modes to lessen their sensed effects. This freedom is taken away from the aircraft system designer when an RSDIMU is implemented since the accelerometers and gyros are colocated. The implication of this restriction must be assessed. However, a complete and thorough study of sensor location and structural mode effects would be extremely complex, involving a detailed consideration of control system stability, phase and gain margins, etc., which is definitely beyond the scope of the present effort. As a compromise, the subjects of sensor location and structural mode effects will be assessed via simulation.

This task is divided into two parts. The first involves the investigation of the effects of sensor location on FDI system performance. The two halves of the RSDIMU are placed at different locations along the vehicle fuselage. The structural mode coefficients are varied with the location of the RSDIMU. The presence of sensor failures is also evaluated. In the second part of this section, the effects of changes in the magnitudes of the structural modes are considered. The absolute values of all of the structural mode coefficients for an RSDIMU cluster are changed by a specified percent. In both cases, the 30 minute flight

59

profile of Table 2 is used. Sensor noise is not considered. The
locations assumed for the RSDIMU clusters are given in Table 10.

5.2   Results of the Sensor Location Parametric Study

The results obtained for the sensor location effects study are
presented in Table 11 for those cases in which sensor failures are not
present. They indicate that the effects of lateral separation are not
significant (Case 4 vs. Case 6). A similar result can be expected when
the sensor clusters are separated in the normal direction since the
structural mode coefficients are only longitudinally dependent. False
alarms occur when at least one half of the RSDIMU is placed at the rear
of the aircraft (Cases 3 and 5). The airplane response also becomes
unstable with both halves of the RSDIMU located far aft of the c.g. This
instability may be due to the destabilizing influence of the pitch rate
feedback term induced by the normal accelerometer lever arm term. False
alarms did not occur in those cases in which the sensors are located
forward of the aircraft c.g.

The results for the cases in which sensor failures are introduced
are summarized in Table 12. Only two locations were considered, FS77 and
FS313. No problems were encountered with the FDI system. For example,
the gyro channel performed perfectly despite the long time it took to
detect the 3.0 deg/hr failure introduced during the loiter maneuver. In
addition, the order in which the sensor failed did not affect the
results.

The analytic compensation of the accelerometer outputs for the
lever arm effects was also evaluated during this phase of the study.
Basically, the lever arm terms of Eqs. (3) and (4) were computed using
the RSDIMU outputs. The angular accelerations were obtained by passing
the RSDIMU angular velocities through washout filters. This approach was
abandoned after simulation evaluation due to the fact that it introduced
false alarms into the system. It was found to be better to include a

Table 10

Location of RSDIMU Clusters Relative to Vehicle c.g.

LOCATION	x-DISTANCE (Meters)	y-DISTANCE (Meters)	z-DISTANCE (Meters)
FS77	6.172	.4572	.3048
FS200	3.048	.4572	.1524
FS313	.1777	∓.4572	0
FS563	-6.172	.4572	-.4572

Table 11

Results of Sensor Location Effects Study - No Failures

CASE	RSDIMU LOCATION (x,y,z Location Of One Half In Meters)	RSDIMU LOCATION (x,y,z Location of Second Half in Meters)	COMMENTS
1	FS313 (.178,.457,0.)	FS313 (.178,.457,0.)	No False Alarm
2	FS313 (.178,-.457,0.)	FS77 (6.172,.457,.3048)	No False Alarm
3	FS313 (.178,-.457,0.)	FS563 (-6.172,.457,-.457)	False Alarm in the Gyro Soft Failure Detection Channel
4	FS77 (6.172,.457,.457)	FS77 (6.172,-.457,.457)	No False Alarm
5	FS563 (-6.172,.457,-.457)	FS563 (-6.172,.457,-.457)	False Alarm in the Gyro Soft Failure Channel-Unstable Aircraft System
6	FS77 (6.172,.914,.457)	FS77 (6.172,-.914,.457)	No False Alarm No Significant Difference From Case 4
7	FS313 (.178,-.457,0.)	FS200 (3.048,.457,.152)	No False Alarm

Table 12
The Effect of Sensor Location on FDI System Performance In the Presence of Failures

RSD IMU LOCATION FIRST HALF	RSD IMU LOCATION SECOND HALF	FAILURE MAGNITUDES						COMMENTS
		ACCELEROMETERS			GYROS			
		Axis #4 at 505 Sec (μg)	Axis #6 at 1010 Sec (μg)	Axis #8 at 1205 Sec (μg)	Axis #8 at 505 Sec (deg/hr)	Axis #6 at 1100 Sec (deg/hr)	Axis #4 at 1605 Sec (deg/hr)	
FS313	FS77	300.0	300.0	400.0	2.0	3.0	2.0	No False Alarms 20 Sec Delay In Detecting Accelerometer Failures 600 Sec Delay In Detecting Second Gyro Failure
FS313	FS313	300.0	300.0	400.0	2.0	3.0	2.0	No False Alarm 600 Sec Delay In Detecting Second Gyro Failure
FS313	FS77	300.0	300.0	400.0	2.0	5.0	2.0	No False Alarm
FS313	FS77	300.0	300.0	400.0	2.0 (Axis #6)	2.0 (Axis #4)	2.0 (Axis #2)	600 Sec Delay In Detecting Third Gyro Failure
FS313	FS77	300.0	300.0	400.0	2.0 (Axis #4)	2.0 (Axis #6)	2.0 (Axis #8)	600 Sec Delay

term in the FDI system thresholds to account for the accelerometer lever arm effects than to analytically compensate the accelerometer outputs for their presence and not account for them in the thresholds. The analytic compensation process introduced high frequency uncertainties into the system due to the differentiation of the angular rates which resulted in false alarms.

5.3 The Effect of the Magnitude of the Structural Modes on FDI System Performance

The results are summarized in Table 13 with the effects of sensor location and changes in the magnitudes of the structural modes presented. Deviations of about 20% from the nominal structural mode coefficients led to a false alarm in the gyro soft failure detection channel. The accelerometer soft failure channel is less sensitive to the structural modes since a false alarm was not induced when their magnitude was increased by 20%.

5.4 Summary and Conclusions

This phase of the study dealt with an investigation of the effects of sensor location on FDI system performance. The results indicate that

- Location of the RSDIMU aft of the vehicle c.g. is neither desirable nor acceptable. However, an assessment of the impact of the RSDIMU on the stability and control of the aircraft system is a complex problem which must be addressed from the integrated systems point of view.

- The effects of lateral and normal separations of the RSDIMU on the FDI process are not very significant.

- The analytic compensation of the accelerometer outputs for lever arm effects resulted in poor FDI system performance and false alarms.

Table 13

The Effect of the Magnitude of the Structural Mode
Coefficients on FDI System Performance

RSDIMU LOCATION FIRST HALF	RSDIMU LOCATION SECOND HALF	PERCENT CHANGE IN FIRST COEFFICIENTS FROM NOMINAL	PERCENT CHANGE IN SECOND HALF MODE COEFFICIENTS FROM NOMINAL	COMMENTS
FS313	FS77	0.	0.	No False Alarm.
FS313	FS77	10.0	0.	No False Alarm
FS313	FS77	21.0	0.	False Alarm in Gyro Soft Failure Detection Channel
FS313	FS77	0.	10.0	No False Alarm
FS313	FS77	0.	21.0	No False Alarm

A second task involved a parametric study of the effects of the magnitude of the structural modes on the FDI system. It was concluded for this phase of the study that

- The gyro channel is more sensitive to variations in the structural modes than the accelerometer channel.

- Structural mode effects which are large relative to the other RSDIMU uncertainties may adversely impact the performance of the FDI algorithm.

SECTION 6

THRESHOLD GENERATION USING NOISE COMPENSATION
AND FILTERED PARITY EQUATION RESIDUALS

6.1   Introduction

The threshold generation scheme used up to this point in the
program is that developed in Section 2 of this report and designated the
least squares estimation approach. The structural mode and accelerometer
level arm threshold effects are obtained by

- calculating a least square estimate of the linear accelerations
  and angular velocities.

- estimating the sensor outputs using these estimated parameters.

- subtracting the actual and estimated sensor signals to obtain
  an estimate of the sensor uncertainties.

- solving the parity equations using these sensor uncertainties.

- using the absolute values of the parity equation residuals
  obtained in the thresholds.

The above defined approach has several shortcomings. In
particular, it does not include noise compensation as developed in
Section 4. Furthermore, the parity equation residuals obtained with this
approach are corrupted by the sensor errors. It has been demonstrated
that the presence of these sensor error effects can lead to false alarms.

6.2   The Reformulated Threshold Algorithm

An alternate approach to threshold generation was explored to overcome these shortcomings. A block diagram of the scheme mechanized is shown in Figure 14. Noise compensation, as developed in Section 4, is included. In addition, the threshold terms, required to compensate for the structural mode effects, are obtained by filtering the parity equation residuals. This approach was recommended by F. Morrell of NASA Langley. The structural mode effects are high frequency in nature. Their frequencies are much higher than those of the bare airframe of the vehicle. The quantity required to compensate for the structural mode effects in the thresholds is given in Eq. (9) and can be obtained exactly by washout or high pass filtering the parity equation residuals.

A slightly different approach is required with the accelerometer lever arm effects. In this case, both low and high frequency compensation must be considered. The high frequencies are important during vehicle transients while the low frequencies are significant during slow maneuvers such as a loiter. The high frequency portions of the lever arm contribution to the threshold are obtained with the high pass filtering of the parity equation residuals. The low frequency portion can be obtained by calculating the accelerometer lever arm effects using the analytic expression of Eq. (4). The angular accelerations required to do this can be obtained by high pass filtering the angular rates. The effect of the low frequency lever arm uncertainties on the individual sensors can be obtained by resolving these uncertainties through the sensor geometry matrix. The lever arm effects required for the thresholds can be obtained by low pass filtering the resultant residues and adding in the high frequency contribution obtained by filtering the parity equations. The low pass and high pass filters used in this process are complementary.

The filtered parity equation approach to threshold generation is not without its potential shortcomings. Specifically, a problem could arise with the acceleration channel when an undetected gyro failure is
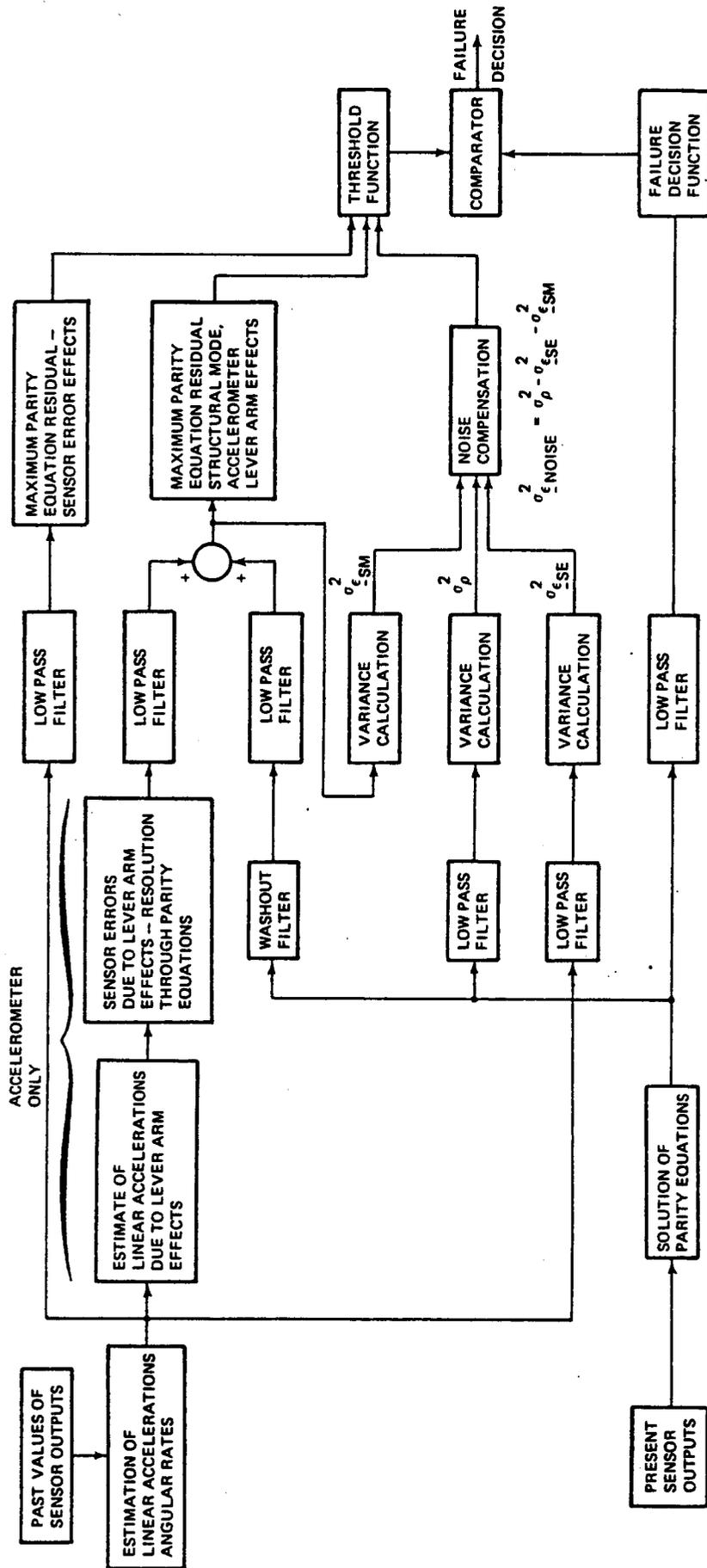
Figure 14. Block Diagram of Failure Detection Process Using Noise Compensation and Filtered Parity Equation Residuals

present. In this instance, the estimated angular rates of the vehicle are corrupted by the gyro failure which, in turn, affects the estimates of the linear acceleration due to the lever arm effects. Since this quantity is low pass filtered the undetected gyro failure affects the threshold. The consequences of its effect cannot be predicted. If the threshold is lowered a false alarm could result or if the threshold is increased the failure could go undetected or a longer detection time could result. The problem just discussed was evaluated via simulation. It was shown to be of only negligible concern for small undetected gyro failure. Large undetected gyro failures affect the vehicle controllability which is a problem of much greater consequence.

The estimates of the gyro and accelerometer structural mode and high frequency lever arm effects required for the thresholds are not affected by an undetected failure. Each of these quantities is obtained by high pass filtering the parity equation residuals and the effects of an undetected failure will not be transmitted.

The noise compensation is not affected by an undetected failure since both σ_ρ and $\sigma_{\varepsilon_{SE}}$ increase to reflect the presence of the failure. $\sigma_{\varepsilon_{SE}}$ is substracted from σ_ρ so that the effect is cancelled out and σ_n is correct.

The effect of an undetected sensor failure on the estimates of the sensor error effects for the threshold is second order in nature. The estimated angular rates or linear accelerations are modified by the nominal estimate of the sensor error which greatly reduced its effect.

6.3   Algorithm Evaluation

The values of the time constants for the washout and low pass filters required for the estimates of the structural mode and lever arm effects for the thresholds were determined via simulation. Noise and sensor error effects were not included and a trial and error approach employed. The washout time constants were selected by comparing time histories of the actual and estimated effects. The low pass filter time

constant for the accelerometer lever arm effects was set equal to that of the high pass filter in complementary filtering fashion. The value of the accelerometer time constants was confirmed for both the structural mode and lever arm effects. For this phase of the study, the RSDIMU was located at FS313 and FS77. Sensor failures were also considered but only the soft failure channel was dealt with.

Based upon the results obtained, washout filter time constants of 15.0 sec and 25.0 sec were selected for the accelerometer and gyros respectively. The accelerometer low pass filter time constant is 15.0 sec. Several tradeoffs are present in the selection of these time constants. If the washout time constants are made larger, the structural mode and high frequency lever arm estimates contain lower frequencies. However, a longer failure detection time results. On the other hand, if the washout filter time constant is smaller, the desired estimates are not adequate and false alarms result. These tradeoffs were evident with the range of simulation runs made to select the filter time constants.

The FDI threshold generation algorithm developed in this section was evaluated in much greater detail. More specifically, the sensitivity of the FDI system performance and the gyro soft failure channel in particular to noise and second order system filter time constant was determined. The results for straight and level flight are presented in Figure 15. Three 2.0 deg/hr failures were injected into the system at 100, 200 and 300 seconds during a 400 sec run. The noise level that can be tolerated increases with the second order filter time constant. A filter time constant that is longer than 40 seconds is not considered, in order to prevent possible masking out of a failure if it occurs immediately after the previous failure or in between maneuvers and also to prevent long detection delay.

Figure 16 shows the performance of the FDI system being evaluated in maneuvering flight. The 1800 second flight profile of Table 2 is used with 2.0 deg/hr failure introduced at 500, 1000 and 1500 sec into sensor
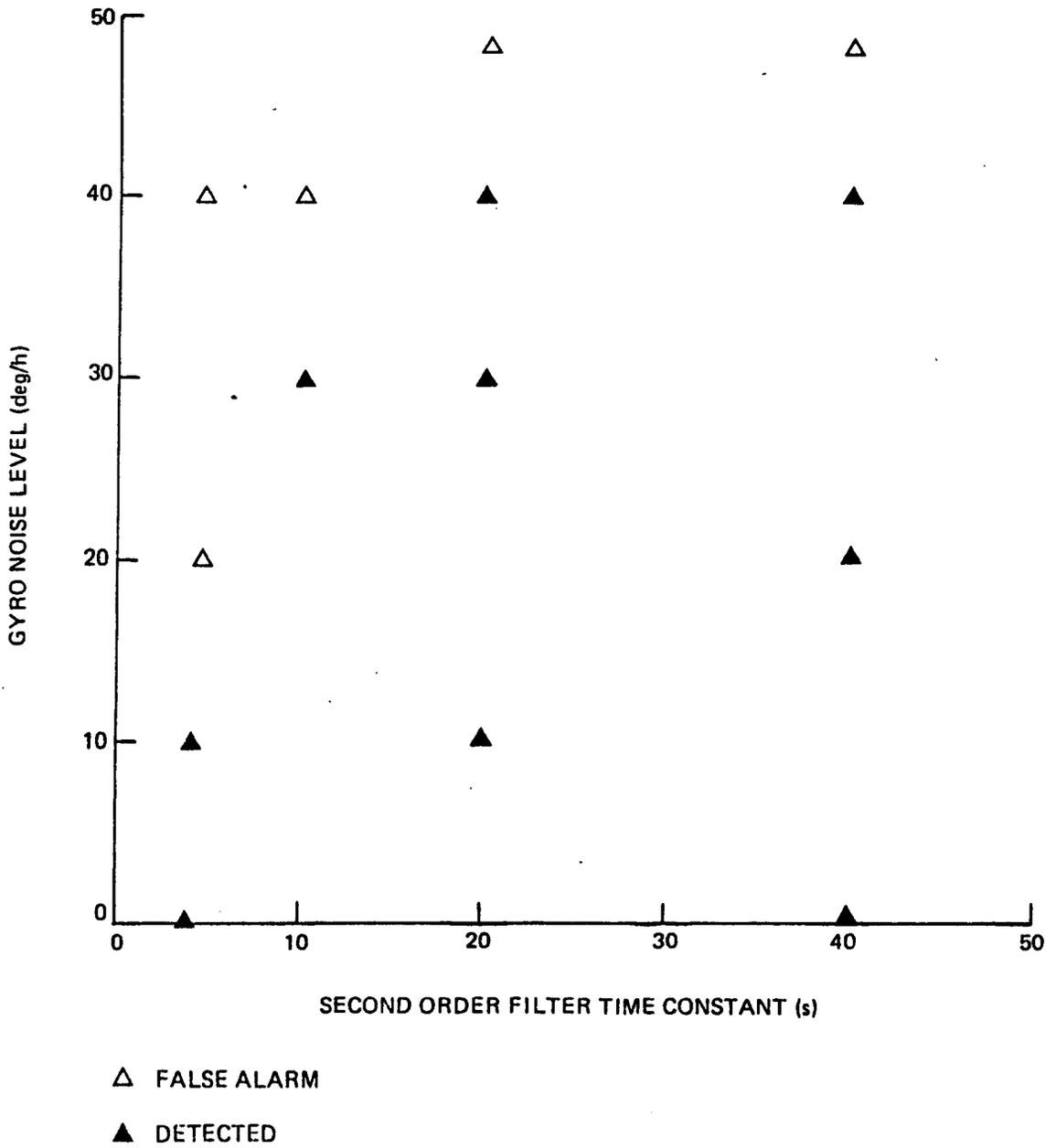
Figure 15. Noise Level vs. Time Constant for Straight, Level Flight, Failure Level 2 Deg/Hr

axes 8, 6 and 4, respectively. The tolerable noise level appears to be linearly related with the time constant between 20 and 40 seconds. The tolerable noise level for this range of time constants is lower than that for straight and level flight.

6.4 A Threshold Algorithm Modification for Reconfiguration

The threshold function, defined in this section, was also modified to account for the memory of the low pass filters associated with it. In the event of failure detection and isolation, the sensor system is reconfigured, the number of parity equations reduced and the threshold function changed to reflect this reduction. This is accomplished by changing a subset of the parity equations and setting others to zero. Step decreases in the threshold function result. It has been observed that after reconfiguration, the detection function can increase before the threshold function can respond to compensate for such effects. The reason for this is that the filters retain some information reflecting the state of the system prior to failure isolation. To prevent false alarms arising because of this phenomena, the threshold function has been modified so that it decays exponentially when a failure is detected and isolated. A time constant of 20 sec has been used for the filter.

The subject of threshold transition after failure detection and isolation is addressed in Figure 17. The failure detection decision function is shown in the top time history. 2.0 deg/hr failures were injected into the system at the times indicated. The middle time history is the gyro threshold without an exponential decay after failure detection and isolation. An instantaneous change in the threshold occurs after the detection and isolation of the second failure which results in a false alarm. The gyro threshold function with an exponential decay after failure isolation is shown in the bottom figure and correct detection and isolation of all three failure occurs.
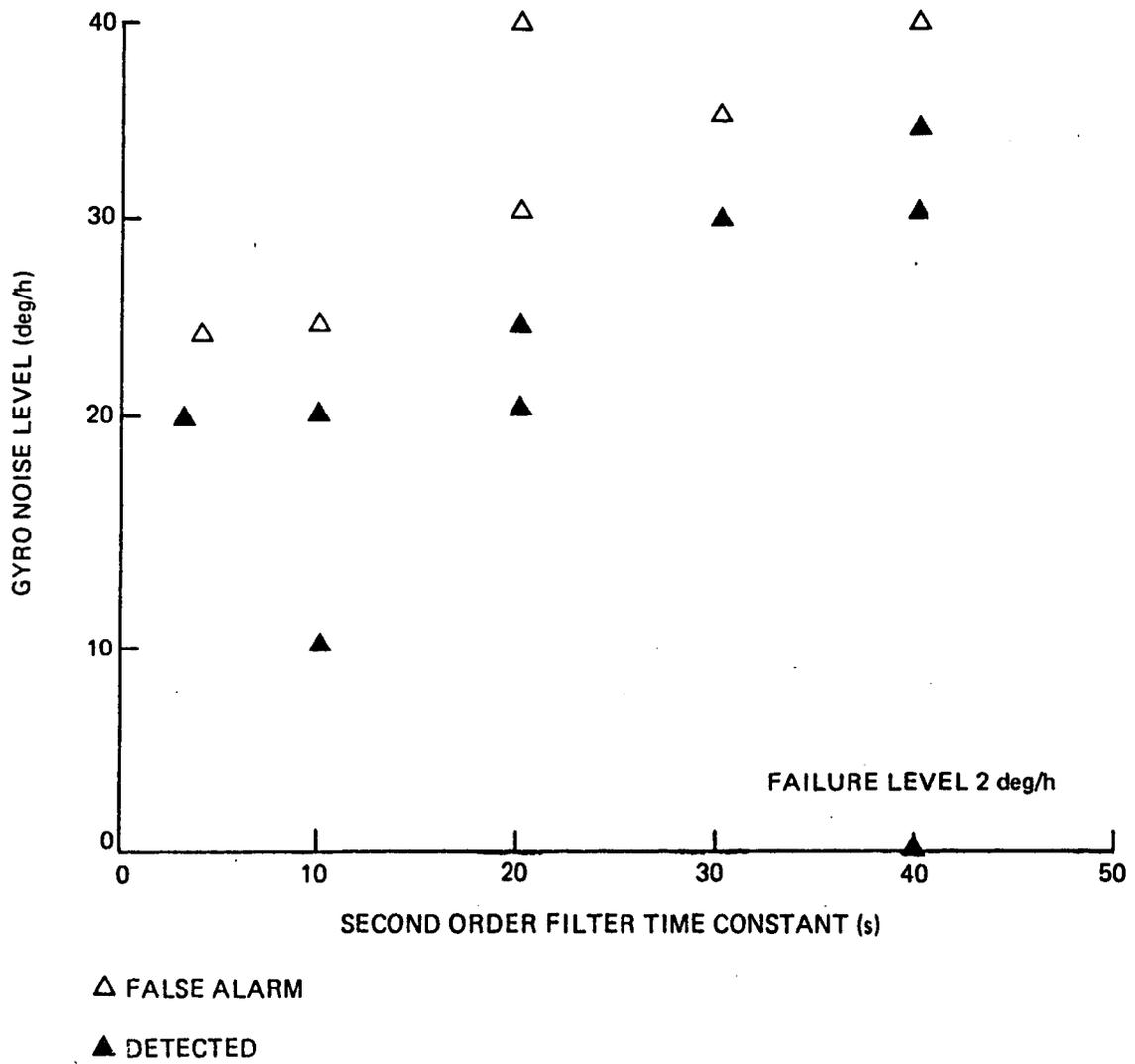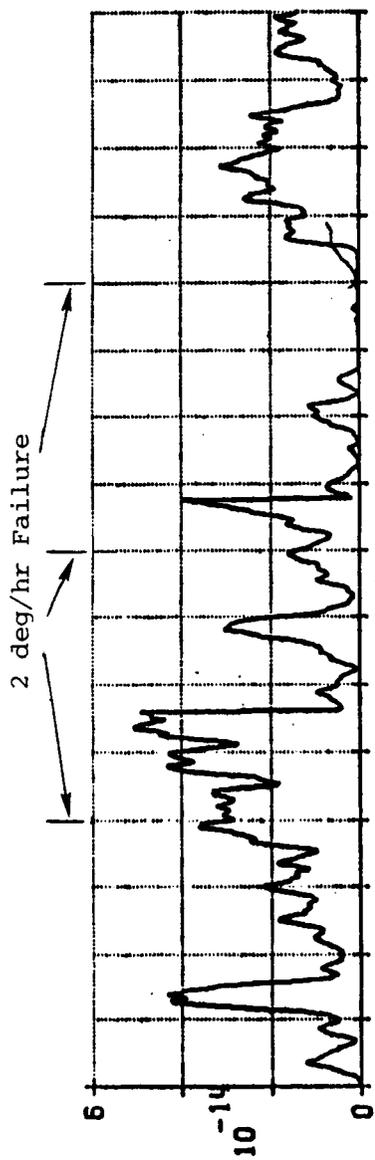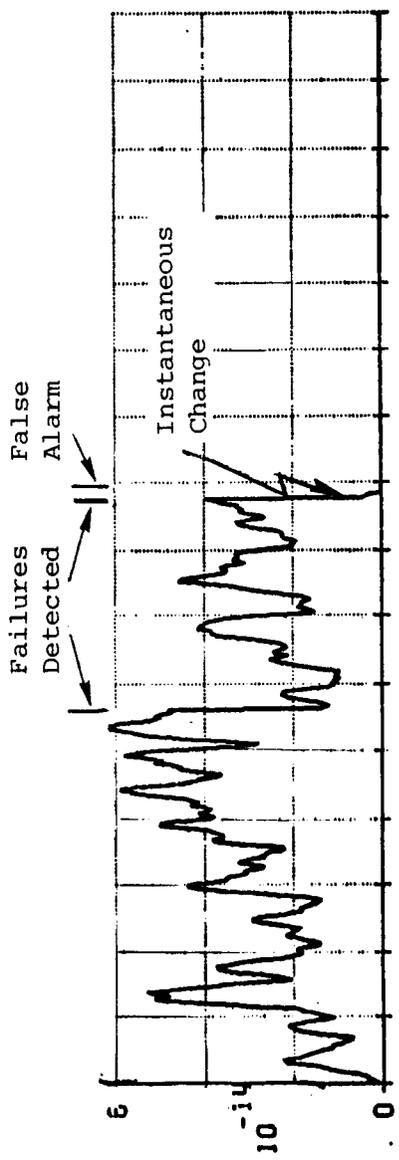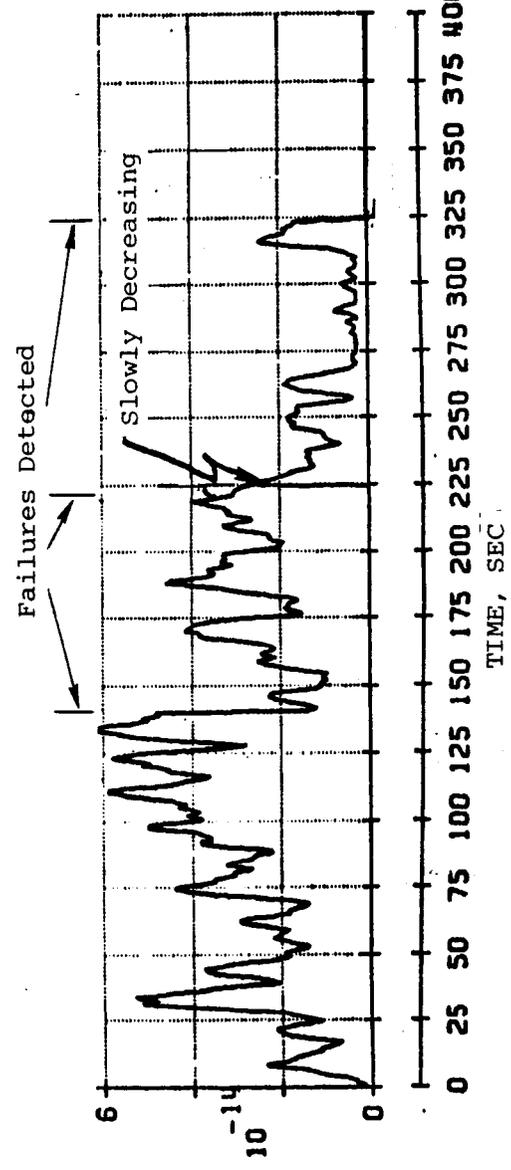
Figure 16. Noise Level vs. Time Constant Maneuvering Flight Profile, Failure Level 2 Deg/hr

Figure 17. Evaluation of Exponentially Decaying Threshold During Reconfiguration

75

6.5   Effect of Sensor Location on Navigation Performance

The reformulated threshold algorithm was also used to evaluate the effect of sensor location on navigation performance. Simulation runs were made using the following locations for the RSDIMU.

- All sensors located near the aircraft center of gravity, FS313

- All sensors located near the front of the fuselage at FS77

- One-half of the RSDIMU at FS313 and the other half at FS77 (nominal case).

Each case was run with and without failures.

Table 14 lists the error ranges for different navigation variables obtained for the 1800 second evaluation run with no failures present. All four sensors were used. The range of error magnitudes is comparable for all combinations of sensor locations. The biggest difference among the error variables for the different locations is that the error trajectories are not equally smooth for all variables. For example, the altitude rate error time history was smoothest when both halves of the RSDIMU are near FS313. A similar difference in smoothness was evident for the yaw angle error. This time, however, the curve is noisiest for all sensors located at FS313. All other navigation error time histories were similar in nature and noise characteristics for all RSDIMU sensor locations.

The simulation run which resulted in Table 14 was repeated with soft accelerometer failures injected into the system to see what influence, if any, this would have on navigation system performance. The failures were detected and correctly isolated. No major differences between the failure and no failure cases were evident.

The effect of sensor location on navigation error when only two sensors are in use was also examined. The outputs of only two sensors will be used for navigation purposes in an operational system so that sensor failures will not affect navigation accuracy. Multiple navigation

Table 14

Maximum Positive and Negative Errors During 1800 Second Evaluation
For Various RSDIMU Sensor Locations - No Failures

NAVIGATION SYSTEM ERROR		SENSOR LOCATION			COMMENTS
VARIABLE	UNIT	FS77-FS77	FS77-FS313	FS313-FS313	
Latitude	degree	(-.00474, .0111)	(-.06384, .0225)	(-.00388, .0249)	No difference in results
Longitude	degree	(0.0, .008)	(0.0, .006)	(0.0, .005)	
Altitude	meter	(-4.188, 3.432)	(-4.088, 3.182)	(-3.972, 3.118)	
North Velocity	m/s	(-.030, 10.224)	(-.0149, 7.785)	(.00024, 6.728)	Altitude rate error smoothest if all sensors at FS313. No difference for other velocity variables.
East Velocity	m/s	(-1.265, 6.122)	(-1.177, 5.668)	(-1.184, 3.873)	
Altitude Rate	m/s	(-.242, .151)	(.231, .169)	(-.198, .130)	
Roll Angle	degree	(-.0833, .0633)	(.0710, .0563)	(-.0578, .0465)	Errors most stable when all sensors are at FS77 for yaw angle only. No difference for other angles.
Pitch Angle	degree	(-.0618, .0695)	(-.0504, .0580)	(-.0463, .0457)	
Yaw Angle	degree	(-.0378, .073)	(-.0313, .0176)	(-.0213, .0095)	

solutions based on all combinations of two sensor outputs will be generated. Only solutions obtained from failure-free sensors are valid. Switching from the failure-contaminated solutions to the failure-free solutions will be part of the system reconfiguration.

Simulation runs were made using the following locations for the sensor pair:

- Two sensors located near the front of the fuselage at FS77.

- One sensor located near the front of the fuselage at FS77 and the other near the aircraft center of gravity at FS313.

- Two sensors located near the center of gravity at FS313.

The results obtained from the simulation runs were compared to each other, as well as to the nominal case, where four sensors were used, two at FS77 and two at FS313. Figure 18 illustrates the results for altitude rate errors. Figure 18b indicates that the error obtained with two sensors at FS77 is even smaller than those obtained for the four sensor nominal case of Figure 18a. The difference in results can be quite large for some variables, as Figure 19 shows for the east velocity error.

The results of Figures 18 and 19, however, represent only a few samples from the spectrum of those possible. CSDL could not draw a general conclusion regarding the preferable location for a sensor pair with regard to navigation system performance. A covariance, rather than a deterministic, approach to the problem is suggested as a preferable way to obtain the desired conclusion.

6.6   Results of Sensor Error Parametric Study on FDI Performance

Attempts to reduce the level of the threshold function derived in Section 6.4 were made in order to improve the soft failure detection capability of the FDI algorithm. The lower the threshold level, however, the higher the probability of false alarm. In order to determine a lower limit on the level of the threshold function, a parametric analysis was conducted in which the sensor error terms represented in the threshold

78

Figure 18. Altitude rate error when only two sensors are used
          in m/s (fps)

a) Nominal Case: Two sensors at FS77, two at FS313.
b) Two sensors at FS77.
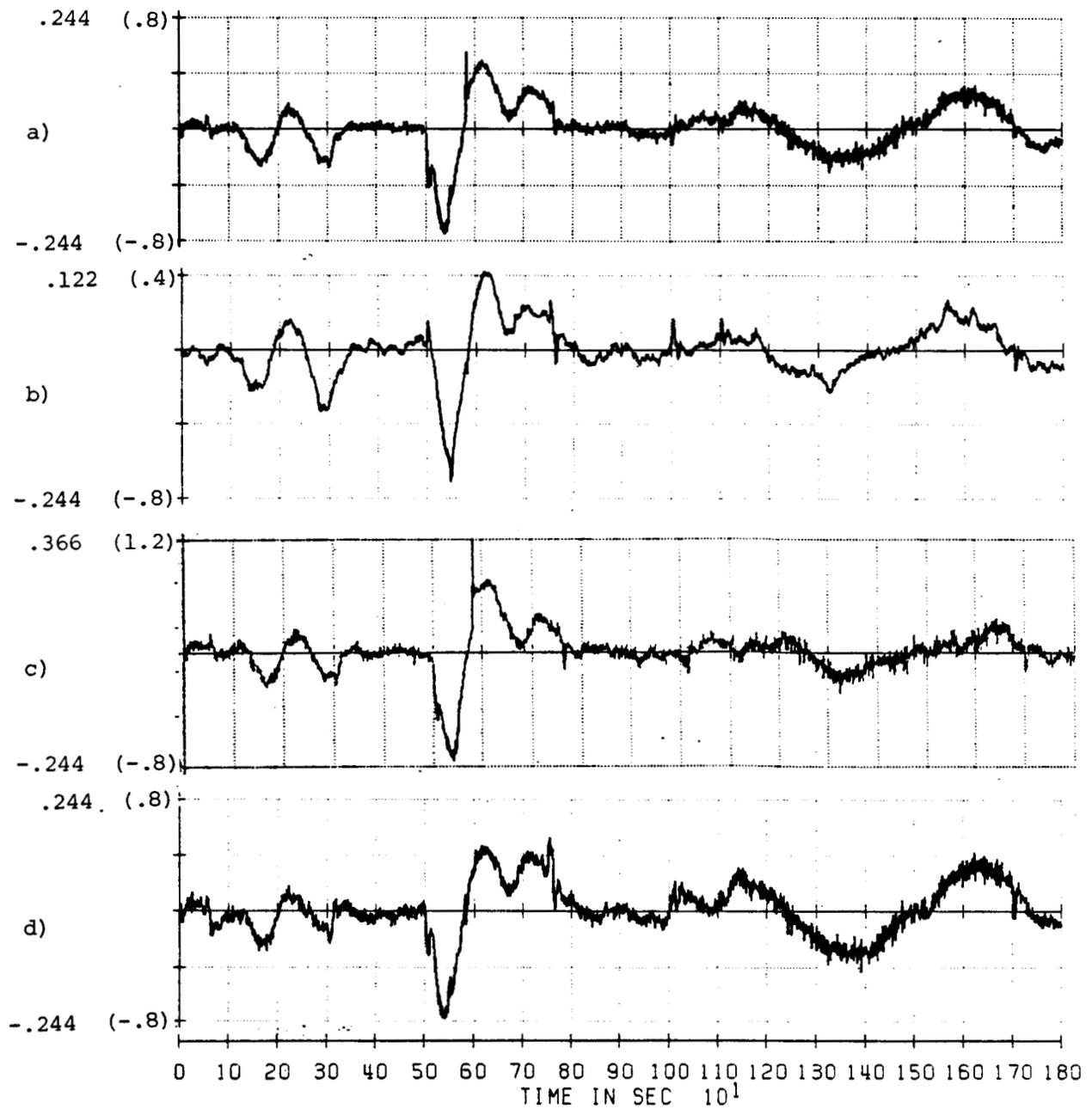c) One sensor at FS77, and one at FS313.
d) Two sensors at FS313.
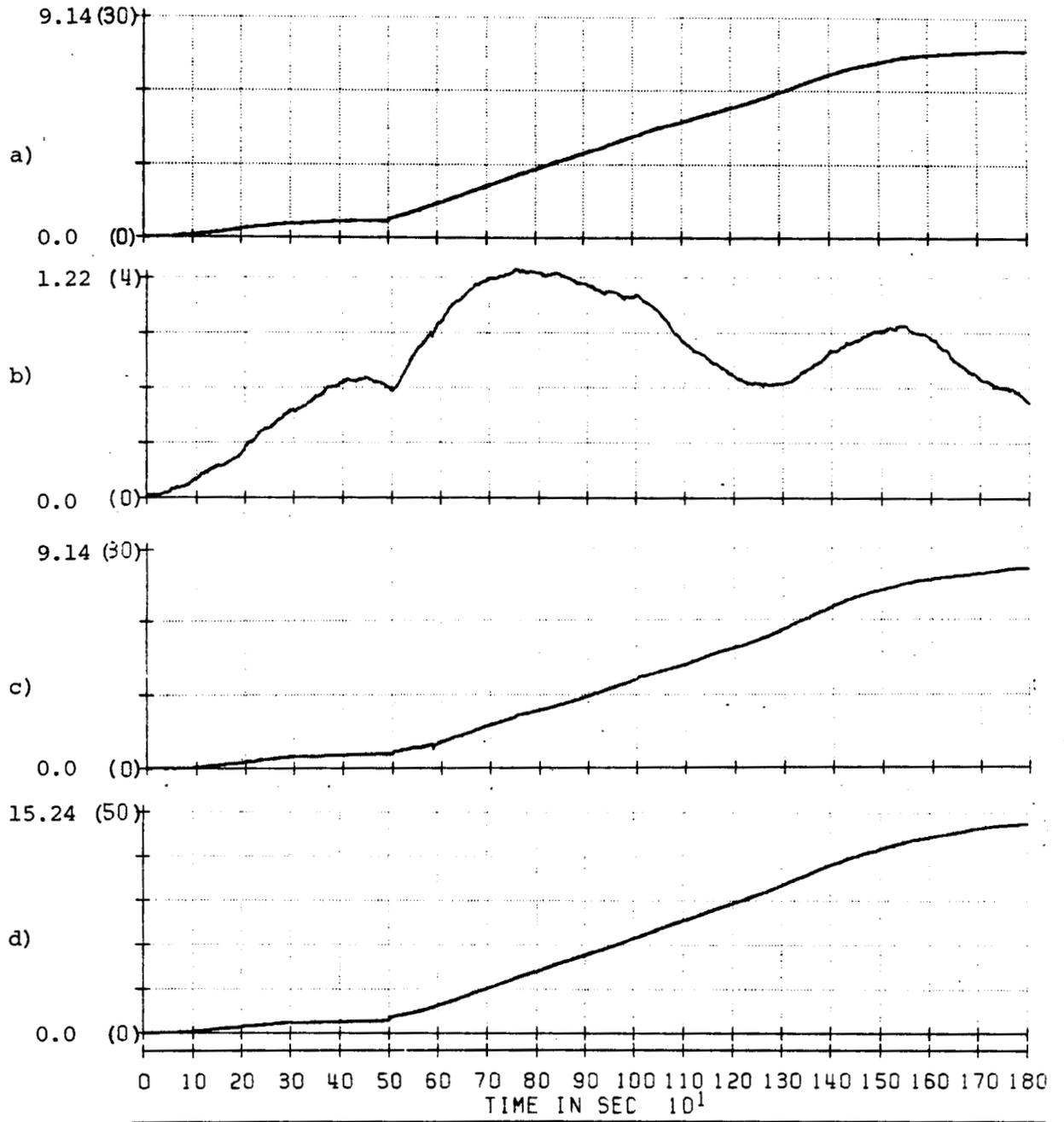
Figure 19. East velocity error when only two sensors are used in m/s (fps)

a) Nominal Case: Two sensors at FS77, two at FS313.
b) Two sensors at FS77.
c) One sensor at FS77, and one sensor at FS313.
d) Two sensors at FS313.

were lowered simultaneously until a false alarm was obtained. For both the accelerometer and gyro sensors, the following error terms were considered:

- instrument bias

- misalignment

- scale factor

- g-sensitivity due to 1-g flight

For the gyros, the g-sensitivity and instrument bias error effect were combined into one term in the threshold since the flight trajectory is nominally 1-g.

The 1800 second simulation trajectory was used in order to examine the effect of maneuvers on lowered threshold levels. The results obtained are shown in Table 15 for the accelerometer and in Table 16 for the gyroscopes. These results indicate how low the threshold level can be set before obtaining false alarms.

The threshold error terms can be lowered significantly from the nominal values. No failures were injected into the simulation runs up to this point. A subset of these runs was, however, repeated with soft accelerometer and gyro failures injected into the system to see whether the results of Tables 15 and 16 were still valid when only two or three sensors are functioning. It was found that the results are indeed repre- sentative for cases with as well as without failures.

6.7   The Effect of Failure Order on FDI Performance

A large number of simulation runs were made to determine whether failing two sensors in different order or at different times affected failure detection and isolation system performance. For this set of experiments, one half of the RSDIMU was placed at the front of the fuselage (FS77) and the other half at the center of gravity (FS313). The

Table 15
Accelerometer Threshold Sensor Error Values
For Parametric Study

ERROR TERM	UNIT	NOMINAL VALUE	LOWEST VALUE WITHOUT FALSE ALARM	FIRST VALUE RESULTING IN FALSE ALARM
Instrument Bias	μg	150.	25.0	18.5
Misalignment	μrad	86.6	21.5	16.5
Scale Factor	ppm	86.6	21.5	16.5
g-sensitivity	μg/g^2	90.	35	31.5

Table 16
Gyro Threshold Sensor Error Values
For Parametric Study

ERROR TERM	UNIT	NOMINAL VALUE	LOWEST VALUE WITHOUT FALSE ALARM	FIRST VALUE RESULTING IN FALSE ALARM
Instrument Bias	deg/hr	0.03	0.0054	0.0045
Misalignment	μrad	150	37.5	32.5
Scale Factor	ppm	60	15	12.5

following simulation runs were made for both the gyros and the acceler-
ometers separately:

- Two sensors at FS77 failed

- One sensor at FS77 and one sensor at FS313 failed

- Two sensors at FS313 failed

For these runs, the 1800 second as well as the all-cruise 500 second
simulation trajectories were used. Two soft failures were introduced
separately for the gyro and the accelerometer during the 1800 second
simulation trajectory, one at 1000 seconds and the other at 1500
seconds. For the 500 second simulation run, they were injected at 150
and 300 seconds. Accelerometer failures of 0.003 g were injected, while
for the gyro the magnitude was 2.0 degrees/hour. In all instances, the
failure order had no effect on either the occurrences of false alarms or
false isolation. All failures were detected and isolated within 25
seconds. Detectability for the second failure, however, varied depending
on which instruments had already been isolated. This issue was discussed
in Reference 1.

6.8   Summary

A reformulation of the FDI system threshold generation algorithm
using noise compensation and filtered parity equation residuals for
structural mode and lever arm effects has been examined. This technique
provides exact compensation of the high frequency structural mode and
lever arm effects in a computationally efficient manner. The low
frequency lever and compensation terms are computed using the angular
velocities computed by the RSDIMU. A shortcoming with this approach was
discussed, which can arise due to the presence of an undetected gyro
failure. Potential consequences of this shortcoming are false alarms or
undetected accelerometer failures. Suitable values for the time
constants of the filters associated with this algorithm were 15 sec for
the accelerometers and 25 sec for the gyros. The performance of the

reformulated FDI threshold generation algorithm was evaluated in the presence of noise as a function of the time constant of the second order low pass filter associated with the gyro soft failure channel. A greater tolerance to noise was indicated with increasing second order filter time constant. Maneuvering flight also decreased the system performance in the presence of noise.

Consideration was also given to the evaluation of an exponential transition in the threshold when reconfiguration of the FDI system occurs. This feature was included to prevent false alarms as indicated by the simulation results included in the report.

An investigation of the effect of sensor location on the navigation performance of the aircraft system with an RSDIMU was presented. Only minor differences were evident. In order to enhance the FDI's soft failure detection capability, a threshold sensor error parametric study was conducted to determine how low the thresholds can be set before false alarms are obtained. Significant reductions can be implemented. Finally, simulation runs were carried in order to determine whether the order in which failures occur has an effect on FDI performance. No difference was evident.

SECTION 7

A GLT FDI SYSTEM STRATEGY BASED ON THE
PAIRWISE COMPARISON OF SENSOR MEASUREMENTS

7.1   Description of the Algorithm

An FDI methodology which combines the detection and isolation
process in one step, is described in this section. Previously, one
parity vector ρ was calculated using a set of eight measurements, output
by four sensors. The detection decision function used, $DF_D = \rho^T \rho$, was
derived based on a Generalized Likelihood Ratio Test and the existence of
a failure was declared if the detection decision function exceeded a
prespecified threshold. Next, the failure was isolated based on the
function DF_{I_j} given by Eq. (2) for each sensor j. The isolation
decision is then made by determining max j (DF_{I_j}). The value of j that
maximizes DF_{I_j} identifies the sensor that is most likely to have failed.

The methodology suggested here is also based on a Generalized
Likelihood Test, but instead of obtaining a single parity vector based on
all measurements, each possible pair of sensors is used to generate one
parity vector, and, in turn, a detection decision function. This gives a
total of $\binom{4}{2}$ = 6 decision functions, each to be compared to a threshold.
Thus, for a pair of sensors i and j, the parity vector ρ_{ij} is defined as

$$\rho_{ij} = [V_{2i-1}, \ V_{2i}, \ V_{2j-1}, \ V_{2j}] \begin{bmatrix} m_{2i-1} \\ m_{2i} \\ m_{2j-1} \\ m_{2j} \end{bmatrix}$$

and the corresponding decision function is

$$DF_{D_{ij}} = \rho_{ij}^T \rho_{ij} \qquad (14)$$

Since each sensor is represented in three decision functions, a decision on whether a failure occurred, and, if so, which sensor to isolate it to, can be made concurrently. Table 17 illustrates this process for a failure in sensor 2. The number of decision functions which exceed the threshold for a sensor j is called the degree of measurement inconsistency of sensor j, or D_j. Thus, as Table 17 indicates, $D_1 = 1$, $D_2 = 3$, $D_3 = 1$, $D_4 = 1$, assuming, of course, that all the GLT tests ran successfully.

In practice, a decision to isolate sensor j is taken if $D_j \geq 2$. Thus, for each sensor pair i,j, define the logical variable

$$F_{ij} = DF_{D_{ij}} > T_{ij} \qquad (i,j = 1,\ldots,4 \; i \neq j)$$

Considering sensor 2, construct the logical expression

$$G_2 = (F_{12} \text{ and } F_{23}) \text{ or } (F_{12} \text{ and } F_{24}) \text{ or } (F_{23} \text{ and } F_{24})$$

If $D_2 \geq 2$, then at least one of the expressions in parentheses in the above equation will be true, which means G_2 will be true or equal to one. For sensor 1, however, $D_1 = 1$, so that $F_{12} = 1$, and $F_{13} = F_{14} = 0$. Thus,

$$G_1 = (F_{12} \text{ and } F_{23}) \text{ or } (F_{12} \text{ and } F_{13}) \text{ or } (F_{13} \text{ and } F_{23})$$

$$= (1.0) + (1.0) + (1.0) = 0$$

To isolate a second failure, given instrument i has failed,

Table 17
Example Illustrating Degree of Inconsistency
For Each Sensor When Sensor 2 is Failed

	SENSOR			
	1	2	3	4
Is $DF_{D_{12}} > T_{12}$?	Yes	Yes	–	–
Is $DF_{D_{13}} > T_{13}$?	No	–	No	No
Is $DF_{D_{14}} > T_{14}$?	No	–	–	No
Is $DF_{D_{23}} > T_{23}$?	–	Yes	Yes	–
Is $DF_{D_{24}} > T_{24}$?	–	Yes	–	Yes
Is $DF_{D_{34}} > T_{34}$?	–	–	No	No.
Degree of sensor inconsistency	$D_1 = 1$	$D_2 = 3$	$D_3 = 1$	$D_4 = 1$

$$G_j = F_{jk}F_{j\ell}$$

where i, j, k, ℓ is a cyclic permutation of 1, 2, 3, 4. That is,

Instrument 1 Failed	Instrument 2 Failed	Instrument 3 Failed	Instrument 4 Failed
$G_2 = F_{23}F_{24}$	$G_1 = F_{13}F_{14}$	$G_1 = F_{12}F_{14}$	$G_1 = F_{12}F_{13}$
$G_3 = F_{23}F_{34}$	$G_3 = F_{13}F_{34}$	$G_2 = F_{12}F_{24}$	$G_2 = F_{12}F_{23}$
$G_4 = F_{24}F_{34}$	$G_4 = F_{14}F_{34}$	$G_4 = F_{14}F_{24}$	$G_3 = F_{13}F_{23}$

In terms of the degree of inconsistency, $D_j = 2$ if sensor j is failed, or $D_j = 1$ otherwise, as shown in Table 18, for the case where sensor 2 was first failed, and sensor 1 failed second.

It can be seen that this algorithm resembles the Edge Vector Test, described in Reference 1, with its overall logic of comparing pairs of sensor measurements. One difference is that the parity equation coefficients, given in Table 19, are derived based on an algorithm, given in Reference 4, which uses a least square approach. More important, the decision function is obtained through a statistical hypothesis test, namely, the GLT. The EVT's decision function, on the other hand, is based on the projection of measurements taken by two sensors along the line of intersection of the same two sensors' planes.

7.2   The Algorithm's Sensitivity to Failures

The orientation of the sensors with respect to the vehicle body axes and the resulting system of parity equations have a profound effect on the magnitude of sensor failures which can be detected and isolated. This aspect of the FDI problem for the redundant IMU sensor configuration and the algorithm under consideration is explored in this section. Single degree-of-freedom instrument failures are assumed because it

Table 18
Example Illustrating Degree of Inconsistency
For Each Sensor When Sensor 1 is Failed,
After Sensor 2 Has Been Correctly Isolated

	SENSOR		
	1	3	4
Is $DF_{D_{13}} > T_{13}$?	Yes	Yes	-
Is $DF_{D_{14}} > T_{14}$?	Yes	-	Yes
Is $DF_{D_{34}} > T_{34}$?	-	No	No
Degree of sensor inconsistency	$D_1 = 2$	$D_3 = 1$	$D_4 = 1$

Table 19
Parity Equation Coefficients
For Pairwise-Comparison GLT Algorithm

	Coefficients of First Sensor		Coefficients of Second Sensor	
	First Axis	Second Axis	First Axis	Second Axis
Adjacent Instruments 1 & 2, 3 & 4, etc.	.68301	.18301	-.18301	-.68301
Two Opposite Sensors 1 & 3, 2 & 4	.5	-.5	.5	-.5

simplifies the discussion and gives insight into the area of FDI sensitivity, and because failure modes of this nature are a distinct possibility with TDOF gyros.

The parity equations attenuate the effect of a sensor failure, thus reducing its magnitude in the parity-equation residuals. To illustrate this fact, consider a failure of magnitude b in Axis A. The measurement m_i would be

$$m_i = \begin{bmatrix} m_{Ai} \\ m_{Bi} \end{bmatrix} = \begin{bmatrix} b \\ o \end{bmatrix} + \begin{bmatrix} \text{Axis } Ai \\ \text{Uncertainties} \\ \text{Axis } Bi \\ \text{Uncertainties} \end{bmatrix}$$

The parity vector is

$$\rho_{ij} = V_{ij}m_{ij} = \begin{cases} .6830b + \text{Residual term} & \text{if } i,j \text{ are adjacent sensors} \\ .5b + \text{Residual term} & \text{if } i,j \text{ are separated sensors} \end{cases}$$

where

$$m_{ij} = \begin{bmatrix} m_{Ai} \\ m_{Bi} \\ m_{Aj} \\ m_{Bj} \end{bmatrix} , \quad V_{ij} = [V_{2i-1}, V_{2i}, V_{2j-1}, V_{2j}], \quad \rho_{ij} = \begin{bmatrix} \rho_{Ai} \\ \rho_{Bi} \\ \rho_{Aj} \\ \rho_{Bj} \end{bmatrix}$$

This failure magnitude is reflected in the decision function as follows:

$$DF_{D_{ij}} = \rho_{ij}^T \rho_{ij} = (V_{ij}m_{ij})^T (V_{ij}m_{ij}) = m_{ij}^T (V_{ij}^T V_{ij}) m_{ij}$$

$$= \begin{cases} (.6830b)^2 + \text{Residual term} & \text{if } i,j \text{ are adjacent} \\ (.5b)^2 + \text{Residual term} & \text{if } i,j \text{ are separated} \end{cases}$$

91

The failure detection sensitivity of sensor i can now be defined as the square root of the coefficient of the term due to failure in the decision function $DF_{D_{ij}}$. This is exactly the same definition used in Reference 1 for the GLT algorithm, where sensitivity is defined as the square root of the sum of the squares of the elements of a column of the parity equation matrices. Table 20 lists these coefficients, where it is seen that uniform detectibility of the first failure does exist with this algorithm, since all of the coefficients obtained for it are permutations of each other. The ability to detect failures degrades for the second and third failures, and the magnitude of failure which can go undetected is larger for three instruments than it is for four. When failure detection for the two-instrument clusters is considered, it is once again evident that a failure larger than that needed in the three- or four-instrument cases has to occur before it is detected. Table 20 shows that the disparity is most evident when, for instance, sensors 1 and 4 are already failed and the third failure occurs in one of the two inner axes of the remaining sensors, namely sensors 2 and 3. In this instance, the failure must be 2.732 times larger than the minimum failure magnitude detected the first time.

7.3   Threshold Selection

The thresholds used with this algorithm can be generated using a method very similar to that used for the GLT algorithm, as described in Section 2.6. They also consist of a constant portion and a dynamic portion. The dynamic thresholds are again generated from an analytic expression for the upper bound of the sensor errors and parity-equation residuals. As with the GLT algorithm, the failure-decision functions are the sum of the squares of the parity-equation residuals, except that sensors are taken two at a time.

Consider the development of the thresholds for a sensor pair i,j. Following Eq. (8), the parity equation residuals is given by

Table 20
Pairwise Comparison GLT Sensitivity Coefficients

FAILED SENSORS	FAILED AXIS	PARITY EQUATION SENSITIVITY COEFFICIENT					
		$\delta DF_{D_{12}}$	$\delta DF_{D_{13}}$	$\delta DF_{D_{14}}$	$\delta DF_{D_{23}}$	$\delta DF_{D_{24}}$	$\delta DF_{D_{34}}$
--	A1	.683	0.5	.183			
	B1	.183	0.5	.683	.683	0.5	
	A2	.183			.183	0.5	
	B2	.683			.183		
	A3		0.5		.683		.683
	B3		0.5				.183
	A4			.683		0.5	.183
	B4			.183		0.5	.683
1	A2				.683		
	B2				.183		
	A3				.183		.683
	B3				.683		.183
	A4						.183
	B4						.683
2	A1			.183			
	B1			.683			
	A3						.683
	B3						.183
	A4			.683			.183
	B4			.183			.683
3	A1	.683		.183			
	B1	.183		.683			
	A2	.183				0.5	.683
	B2	.683				0.5	.183
	A4			.683		0.5	.183
	B4			.183		0.5	.683
4	A1	.683	0.5				
	B1	.183	0.5				
	A2	.183			.683		
	B2	.683			.183		
	A3		0.5		.183		
	B3		0.5		.683		
1,2	A3						.683
	B3						.183
	A4						.183
	B4						.683
1,3	A2					0.5	
	B2					0.5	
	A4					0.5	
	B4					0.5	
1,4	A2				.683		
	B2				.183		
	A3				.183		
	B3				.683		
2,3	A1			.183			
	B1			.683			
	A4			.683			
	B4			.183			
2,4	A1		0.5				
	B1		0.5				
	A3		0.5				
	B3		0.5				
3,4	A3	.683					
	B3	.183					
	A4	.183					
	B4	.683					

93

$$\rho_{ij} = \sum_{k=1}^{4} V_{k_{ij}} \delta m_{k_{ij}} + \text{structural mode terms} \qquad \begin{array}{l} i,j = 1,\ldots,4 \\ i \neq j \end{array}$$

An upper bound for ρ_{ij} is, as in Eq. (9)

$$\rho_{m_{ij}} = \delta m_{m_{ij}} \left(\sum_{k=1}^{4} \left| V_{k_{ij}} \right| \right) + \left| \text{structural mode terms} \right|$$

Given the failure decision function $DF_{D_{ij}}$ of Eq. (14), the upper bound for $DF_{D_{ij}}$ is

$$T_{ij} = \left(\rho_{m_{ij}} \right)^2$$

The constant portion of the threshold is added to this when it is necessary to account for quantization and sensor noise as in the hard-failure channel.

One additional important conclusion can be drawn regarding the thresholds determined for the GLT. The thresholds are not a function of the number of instruments in the configuration. This means that the lower failure-detection sensitivity evident in Table 20 for a configuration with fewer sensors in the cluster is not compensated for by a corresponding lowering of the failure-detection thresholds.

7.4   Simultaneous Failures

This section considers the effect of simultaneous failures on the pairwise-comparison GLT algorithm. Simultaneous failures can occur, for instance, if a sensor is physically damaged, so that the two axes of that sensor would show corrupt measurements. In a tetrahedral RSDIMU with two separable halves, two sensors, i.e., four measurements, can become invalid at the same instant if damage occurs in that area of the airplane

where that half is located. In this section, cases with only two simultaneous failures will be considered.

As an example, consider the case where the two axes of sensor 1 fail, axis A with magnitude b_1, and axis B with magnitude b_2. The effect on decision function $DF_{D_{12}}$ will be

$$DF_{D_{12}} = \rho_{12}^T \rho_{12} = \left(V_{12}m_{12}\right)^T\left(\dot{V}_{12}m_{12}\right) = m_{12}^T V_{12}^T V_{12} m_{12}$$

$$= (.6830b_1 + .1830b_2)^2 + \text{Residual term}$$

The effect on decision functions $DF_{D_{13}}$ and $DF_{D_{14}}$ is, respectively,

$$DF_{D_{13}} = .25(b_1 - b_2)^2 + \text{Residual term}$$

$$DF_{D_{14}} = (.1830b_1 + .6830b_2)^2 + \text{Residual term}$$

This means that the effect on the two adjacent sensors is superadditive, and that on the one opposite sensor is subadditive. Since it is sufficient to have two decision functions crossing the threshold, sensor 1 will be detected and correctly isolated.

Consider now the case where the A axis of both sensor 1 and sensor 2 has failed, the first with a failure magnitude b_1 and the second with a failure magnitude b_2, both failures being in the positive direction. The effect on each of the decision functions is listed in Table 21. It is seen that the effect on $DF_{D_{12}}$ is subadditive, so that if, for instance, $b_2 = (.6830/.1830)b_1$, no effect will be seen at all. Table 22 shows that the algorithm cannot handle such a case. If $DF_{D_{12}}$ fails to cross the threshold, the degree of inconsistency of each of the four sensors will be 2, and with the algorithm as it is, all four sensors will be isolated.

Table 21
Effects of a Failure of Axis A
in Each of Sensors 1 and 2 on Decision Functions

	FAILURE OF MAGNITUDE b_1 ON A AXIS IN SENSOR 1 ALONE	FAILURE OF MAGNITUDE b_2 ON A AXIS IN SENSOR 2 ALONE	FAILURE OF MAGNITUDE b_1 on A AXIS OF SENSOR 1 AND OF MAGNITUDE b_2 ON A AXIS OF SENSOR 2
$\delta DF_{D_{12}}$	$(.6830b_1)^2$	$(.1830b_2)^2$	$(.6830b_1 - .1830b_2)^2$
$\delta DF_{D_{13}}$	$(.5b_1)^2$	0	$(.5b_1)^2$
$\delta DF_{D_{14}}$	$(.1830b_1)^2$	0	$(.1830b_1)^2$
$\delta DF_{D_{23}}$	0	$(.6830b_2)^2$	$(.6830b_2)^2$
$\delta DF_{D_{24}}$	0	$(.5b_2)^2$	$(.5b_2)^2$
$\delta DF_{D_{34}}$	0	0	0

Table 22
Degree of Inconsistency for Each Sensor
When Sensors 1 and 2 are Failed

DECISION FUNCTION	SENSOR			
	1	2	3	4
Is $DF_{D_{12}} > T_{12}$?	Yes or No	Yes or No		
Is $DF_{D_{13}} > T_{13}$?	Yes		Yes	
Is $DF_{D_{14}} > T_{14}$?	Yes			Yes
Is $DF_{D_{23}} > T_{23}$?		Yes	Yes	
Is $DF_{D_{24}} > T_{24}$?		Yes		Yes
Is $DF_{D_{34}} > T_{34}$?			No	No
Degree of Sensor Inconsistency	$D_1 = 3$ or 2	$D_2 = 3$ or 2	$D_3 = 2$	$D_4 = 2$

The last example above illustrates a limitation of the algorithm which occurs whenever two different sensors fail simultaneously, and the failures are in the same direction and of comparable magnitude. If b_1 is much larger than b_2, or vice versa, for instance if $b_1/b_2 > 5$ or $b_2/b_1 > 5$, then the failures will not be totally masked and the chances are improved that correct isolation will occur. For this reason, the algorithm must be constructed so that a degree of inconsistency $D_j = 3$ is required if $D_j = 2$ for more than one sensor j. This will prevent the simultaneous isolation of more than two sensors. Finally, Figure 20 shows a flow diagram of the modified algorithm.

7.5   Conclusion

A new FDI system strategy for failure detection and isolation has been presented in this section. The following conclusions regarding this methodology can be drawn from this phase of the study:

- The algorithm offers a concrete strategy for dealing with two simultaneously occurring failures.

- Limitations on this capability do exist, as described in Section 7.4.

- It is still premature to consider this FDI as a potential alternative to the original GLT algorithm, since experience through simulation is still needed. The strategy is, however, worth pursuing further.

m

| $DF_{D_{12}}$ | $DF_{D_{13}}$ | $DF_{D_{14}}$ | $DF_{D_{23}}$ | $DF_{D_{24}}$ | $DF_{D_{34}}$ |
| $\leq T_{12}$ | $\leq T_{13}$ | $\leq T_{14}$ | $\leq T_{23}$ | $\leq T_{24}$ | $\leq T_{34}$ |

DEGREE OF INCONSISTENCY
D_j FOR EACH SENSOR j
j = 1, 4

$D_j \geq 2$
j = 1, 4
FOR ONLY
ONE SENSOR

YES

ISOLATE
SENSOR

NO

$D_j = 3$
FOR 1 OR 2
SENSORS
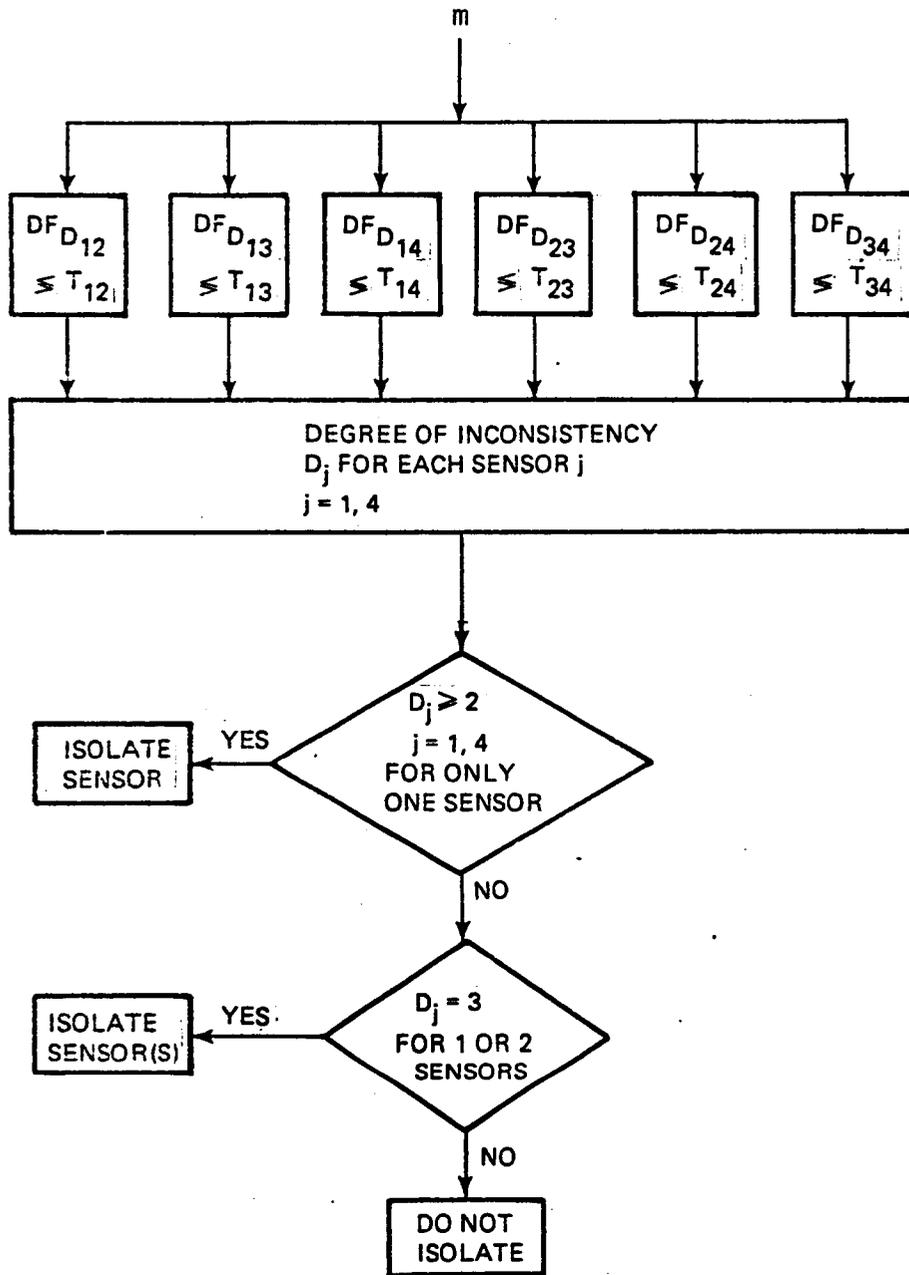
YES

ISOLATE
SENSOR(S)

NO

DO NOT
ISOLATE

Figure 20. Flowchart for Pairwise Comparison Algorithm

SECTION 8

SUMMARY AND CONCLUSIONS

The basic goal of this study effort was to further develop and refine the technical knowledge and skills needed to make redundant strapdown inertial measurement units a viable component of the aircraft avionics system inventory. This study was specifically addressed to the RSDIMU being developed and evaluated by the NASA Langley Research Center. Two major tasks were undertaken: Aeroelastic Effects Analysis and Failure Decision Function Compensation Analysis.

In Section 3, compensated and uncompensated GLT FDI algorithm decision functions were compared. The intent was to determine if the compensated GLT decision functions could be employed to eliminate the need for the dynamic FDI thresholds required with the uncompensated decision functions. The compensated decision function was very sensitive to the variance of the sensor errors, implying that constant thresholds can only be obtained if these parameters are known accurately for a given sensor package. In addition, failures tended to be masked during maneuvers. On the other hand, the algorithm was quite sensitive to soft sensor failures and the approach deserves further consideration.

The investigation of the compensated GLT decision function provided a basis from which to consider the compensation of noise in the GLT thresholds. This compensation is required to eliminate false alarms which can arise if noise effects are not taken into account. An algorithm to achieve noise compensation was developed, implemented and evaluated. An investigation of the impact of the FDI system low pass filter time constant on system performance with noise present was also

conducted. It was concluded that noise compensation is still required even though larger filter time constants lessen the detrimental effects of noise.

An important consideration in the design of RSDIMUs is the impact of sensor location and magnitude of the structural modes on FDI system performance. This subject was addressed in Section 5. It was determined that location of the sensors aft of the vehicle c.g. is not desirable, that lateral and normal separation of the RSDIMU are not significant and that analytic compensation of the accelerometer outputs for lever arm effects inhibits FDI system performance.

An FDI system threshold generation scheme was developed and evaluated in Section 6. This algorithm incorporated noise compensation and filtered parity equation residuals. The filtering of the parity equation residuals provided a means of obtaining the exact compensation of the high frequency structural modes and lever arm effects required for the thresholds. This algorithm was evaluated for different noise levels and second order filter time constants in both cruise and maneuvering flight. A brief investigation of the effects of RSDIMU sensor location on navigation system performance was conducted. In order to enhance the FDI's system soft failure detection capability, a sensor error parametric study was conducted to determine how low the threshold can be set without obtaining false alarms. Simulation runs were also carried in order to determine whether the different orders in which failures can be injected have different effects on FDI system performance. No difference was evident.

A GLT FDI system strategy based on the pairwise comparison of sensor measurements was described in Section 7. The advantage of this strategy is its ability to detect two simultaneously occurring failures, although limitations do exist on this capability.

SECTION 9

REFERENCES

1. Motyka, P., Landey, M., McKern, R., "Failure Detection and Isolation Analysis of a Redundant Strapdown Inertial Measurement Unit," NASA Contractor Report 165658, February 1981.

2. Motyka, P., "Reliability Analysis and Fault-Tolerant System Development for a Redundant Strapdown Inertial Measurement Unit," NASA Contractor Report 166050, March 1983.

3. Hall, S.R., "Parity Vector Compensation For FDI," MIT M.S. Thesis, February 1982. (Also Charles Stark Draper Laboratory Report CSDL-T-763.)

4. Potter, J.E. and Suman, M.C., "Thresholdless Redundancy Management with Arrays of Skewed Instruments," Integrity in Electronic Flight Control Systems, AGARDograph-0224, 1977, pp. 15-1 to 15-25.

1. Report No. NASA CR-172426	2. Government Accession No.	3. Recipient's Catalog No.
4. Title and Subtitle FAULT-TOLERANT SYSTEM CONSIDERATIONS FOR A REDUNDANT STRAPDOWN INERTIAL MEASUREMENT UNIT		5. Report Date August 1984
		6. Performing Organization Code
7. Author(s) P. Motyka, R. Ornedo, R. Mangoubi		8. Performing Organization Report No. CSDL-R-1717
9. Performing Organization Name and Address The Charles Stark Draper Laboratory, Inc. 555 Technology Square Cambridge, Massachusetts 02139		10. Work Unit No.
		11. Contract or Grant No. NAS1-16887
12. Sponsoring Agency Name and Address National Aeronautics and Space Administration Washington, D.C. 20546		13. Type of Report and Period Covered Final Report March 1983 – June 1984
		14. Sponsoring Agency Code 505-34-13-12

15. Supplementary Notes

Langley Technical Monitor: Frederick R. Morrell

16. Abstract

The development and evaluation of a fault-tolerant system for the Redundant Strapdown Inertial Measurement Unit (RSDIMU) being developed and evaluated by the NASA Langley Research Center was continued. The RSDIMU consists of four two-degree-of-freedom gyros and accelerometers mounted on the faces of a semi-octahedron which can be separated into two halves for damage protection. Compensated and uncompensated fault-tolerant system failure decision algorithms were compared. An algorithm to compensate for sensor noise effects in the fault-tolerant system thresholds was evaluated via simulation. The effects of sensor location and magnitude of the vehicle structural modes on system performance were assessed. A threshold generation algorithm, which incorporates noise compensation and filtered parity equation residuals for structural mode compensation, was evaluated. The effects of the fault-tolerant system on navigational accuracy were also considered. A sensor error parametric study was performed in an attempt to improve the soft failure detection capability without obtaining false alarms. Also examined was an FDI system strategy based on the pairwise comparison of sensor measurements. This strategy has the specific advantage of, in many instances, successfully detecting and isolating up to two simultaneously occurring failures.

17. Key Words Suggested by Author Failure Detection and Isolation Redundant Inertial Measurement Unit	18. Distribution Statement Unclassified – Unlimited Subject Category – 04

19. Security Classif. (of this report) Unclassified	20. Security Classif. (of this page) Unclassified	21. No. of Pages 103	22. Price